nature chemistry

Article

https://doi.org/10.1038/s41557-023-01246-6

Reversible 2′-OH acylation enhances RNA stability

Received: 23 March 2022

Accepted: 19 May 2023

Published online: 26 June 2023

Check for updates

Linglan Fang[1], Lu Xiao[1], Yong Woong Jun[1], Yoshiyuki Onishi[1] & Eric T. Kool[1,2]

The presence of a hydroxyl group at the 2′-position in its ribose makes RNA susceptible to hydrolysis. Stabilization of RNAs for storage, transport and biological application thus remains a serious challenge, particularly for larger RNAs that are not accessible by chemical synthesis. Here we present reversible 2′-OH acylation as a general strategy to preserve RNA of any length or origin. High-yield polyacylation of 2′-hydroxyls ('cloaking') by readily accessible acylimidazole reagents effectively shields RNAs from both thermal and enzymatic degradation. Subsequent treatment with water-soluble nucleophilic reagents removes acylation adducts quantitatively ('uncloaking') and recovers a remarkably broad range of RNA functions, including reverse transcription, translation and gene editing. Furthermore, we show that certain α-dimethylamino- and α-alkoxy- acyl adducts are spontaneously removed in human cells, restoring messenger RNA translation with extended functional half-lives. These findings support the potential of reversible 2′-acylation as a simple and general molecular solution for enhancing RNA stability and provide mechanistic insights for stabilizing RNA regardless of length or origin.

The thermal and enzymatic instability of RNA presents profound challenges to RNA vaccines and therapies, imposing severe limits on RNA analysis, storage and transportation, and also on pharmacology[1,2]. RNA degradation is pervasive and arises both from spontaneous thermal degradation and from the action of adventitious ribonuclease enzymes[3]. RNA in-line hydrolysis starts with the attack of the deprotonated 2′-hydroxyl group on the vicinal 3′-phosphate, coordinated with the departure of the adjacent 5′-alcohol group and resulting in a 2′,3′-cyclic phosphate (Fig. 1a)[3,4]. The same mechanism, aided by general acids and bases in the ribonuclease active site, also underlies RNA premature degradation by nuclease enzymes (for example, ribonucleases (RNases)) that are ubiquitously present in cells and biofluids[2,5], limiting half-lives of bioactive RNAs employed in therapeutic strategies[6,7].

Current methods to preserve RNA include the incorporation of modified inter-nucleotide linkages[8,9], chemically altered nucleotides[10–12], modified ribose[13] and structure-guided sequence design[7]. While these chemical modifications and sequence optimization have been widely employed to enhance RNA stability, their broad application is chiefly limited to short chemically synthesized RNA and can impart significant labour and expenses (Fig. 1b). Therefore, finding cost-effective strategies to preserve and subsequently restore RNA of any origin post-synthetically under mild conditions could constitute a major advance in RNA technologies in general and facilitate the storage and therapeutic use of a broad range of biologically active RNAs.

RNA degradation could in principle be blocked by post-synthetic acylation of 2′-hydroxyl groups in RNA (Fig. 1c). Indeed, a recent study observed that 2′-acylation can protect a short synthetic RNA against recombinant RNases[14]. However, the broad use of such modification for RNA protection is hindered by a lack of high-yield biocompatible reversal strategies and a limited understanding of how the origin, length and structure of an RNA influence its stability when acylated. In addition, no data have been reported on the effects of acylation on messenger RNAs (mRNAs) and their translation in cells.

Numerous chemical reagents, such as anhydrides and acyl chlorides, have been described for 2′-hydroxyl covalent modification[15–17]. However, the short aqueous half-lives and poor water solubility of

[1]Department of Chemistry, Stanford University, Stanford, CA, USA. [2]Sarafan ChEM-H Institute, Stanford University, Stanford, CA, USA.
e-mail: kool@stanford.edu

https://doi.org/10.1038/s41557-023-01246-6

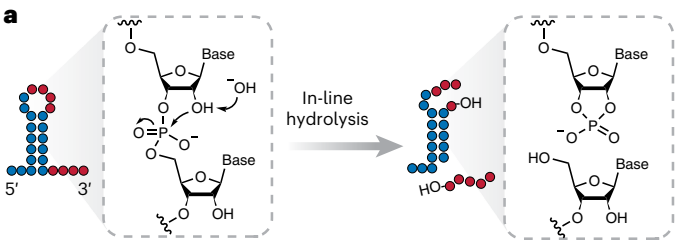

b

	Previous methods	This study
Modification	For example, 2′-F, 2′-OMe, PS	2′-OH acylation
Incorporation	During synthesis	Post-synthetic
RNA length	Only short RNAs	Any length
RNA origin	Only synthetic RNA	Any origin
Reversibility	Irreversible	Reversible

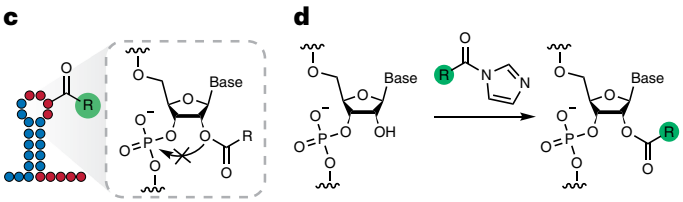

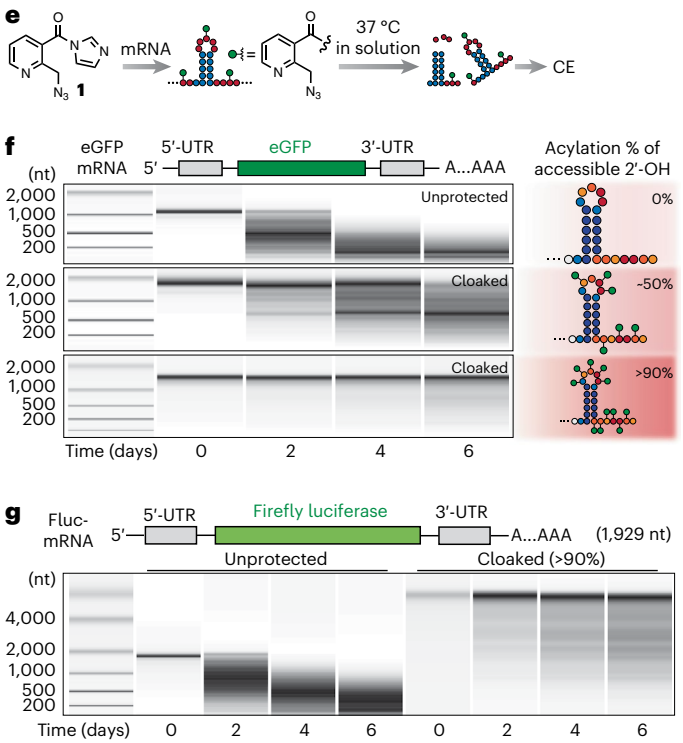

Fig. 1 | RNA polyacylation (cloaking) inhibits thermal degradation of RNA. **a**, Molecular mechanism of RNA thermal degradation in solution. Nucleotides with unstable and stable 3′-phosphodiester bonds are coloured red and blue, respectively. **b**, Comparison of existing RNA chemical modifications to this study. PS, phosphorothioate. **c**, RNA with acylated 2′-hydroxyls in riboses resists thermal degradation by blocking nucleophilic 2′-hydroxyls from attacking the vicinal 3′-phosphodiester bonds. **d**, Acylimidazole reagents selectively acylate 2′-hydroxyls of RNA in high yields in aqueous solutions. **e**, Workflow of accelerated mRNA ageing assay to determine thermal stability (water, 37 °C) of mRNA cloaked with NAI-N_3 (**1**) with CE analysis. **f**,**g**, The apparent RNA quality (measured by CE) of eGFP-mRNA (**f**) and Fluc-mRNA (**g**) cloaked with **1** upon incubation in RNase-free water over time. **f**, eGFP-mRNA (996 nt) tested was unprotected (top), with ~50% (middle) or >90% (bottom) of unpaired accessible 2′-hydroxyls cloaked with **1**. The background colour density indicates the extent of cloaking. **g**, Fluc-mRNA (1,929 nt) tested was either unprotected (left) or extensively (>90%) cloaked (right) with **1**. Data shown are images of CE traces. The experiments in **f** and **g** were conducted twice ($n = 2$) with similar results. Note: cloaking reduces the electrophoretic mobility of mRNA. UTR, untranslated region.

reagents with these functional groups limit the extent of RNA modification. More recently, two chemotypes have been developed to overcome these issues; alkylamino-substituted isatoic anhydrides[18,19] and acylimidazoles[20,21] can survive longer in water and react in high yields with RNA. We were attracted to acylation by acylimidazoles due to their simplicity, ease of preparation, high water solubility and their effective RNA 2′-polyacylation ability (Fig. 1d). We recently demonstrated that acylimidazoles can efficiently react with 2′-hydroxyls rather than exocyclic amines on nucleobases[22] and exhibit tunable hydrolytic half-lives[23]. Acylimidazoles are easily accessible by one-step activation of the corresponding carboxylic acids with equimolar 1,1′-carbonyldiimidazole. Moreover, the 2′-carboxyl ester adducts with RNA can be reversed by design, offering a possible solution to reinstate unmodified 2′-hydroxyls[22–25]. These properties led us to consider the possibility that acylimidazoles might offer a simple solution to reversibly functionalize 2′-hydroxyls and block RNA degradation before biological use.

In this Article, we demonstrate that reversible 2′-hydroxyl acylation by designed acylimidazole reagents can broadly protect RNA from thermal and enzymatic degradation. The regioselective, high-yield reaction between 2′-hydroxyls and water-soluble acylimidazoles ('cloaking') affords 2′-polyacylation of a wide range of RNAs, ranging from short synthetic RNAs to long endogenous mRNAs. Using a set of readily accessible acylimidazoles that are structurally diversified, we surveyed how 2′-polyacylation of RNA influences its thermal and enzymatic instability. Further, we describe the discovery of water-soluble nucleophilic reagents that can efficiently remove selected acylation adducts ('uncloaking') and restore RNA functions, including reverse transcription, translation and gene editing. Finally, we report that certain acylation adducts are reversed spontaneously in cells and restore mRNA translation with extended functional half-lives. Taken together, our reversible acylation reagents and methods represent a simple and broadly applicable post-synthetic strategy to preserve and subsequently recover RNA activity, which is otherwise not achievable by existing chemical modifications of RNAs (Fig. 1b).

Results and discussion

RNA cloaking shields RNA from thermal degradation

RNAs (particularly longer RNAs) are susceptible to chain cleavage in water accelerated by thermal motions[26,27]. No report has yet shown how high levels of 2′-modifications (for example, 2′-F and 2′-OMe) affect the stability of long RNAs (>600 nucleotide(s) (nt)), in large part because these modifications cannot be efficiently incorporated into RNAs with lengths beyond ~150 nt in synthetically accessible yields[28]. Thus, we first prepared a 2′-polyacylated ('cloaked') model mRNA by reacting a well-studied enhanced green fluorescent protein (eGFP)-mRNA (996 nt) with NAI-N_3 (**1**), an acylimidazole reagent known to selectively acylate 2′-hydroxyls in high yields (Fig. 1e)[21]. Matrix-assisted laser desorption/ionization–time of flight (MALDI–TOF) analysis with an 18 nt unstructured RNA determined reaction conditions that provide intermediate (~50%) and extensive (>90%) cloaking in unpaired accessible regions of RNA (Extended Data Fig. 1 and Supplementary Table 1). These conditions were used to generate modified eGFP-mRNA with an estimated 50% or nearly 90% of unpaired accessible 2′-hydroxyls

cloaked by **1**. Cloaking by **1** leads to the reduced electrophoretic mobility of eGFP-mRNA (Supplementary Fig. 1).

As an initial assessment of how cloaking affects the stability of RNA, we performed accelerated RNA-ageing experiments by incubating eGFP-mRNA species with or without cloaking in RNase-free water at a mildly elevated temperature (37 °C) (Fig. 1e). We then evaluated the lifespan of the mRNA by measuring the relative fraction of remaining fully intact RNA over time. Analysis by capillary electrophoresis (CE) of RNA fragments showed cloaking-dependent resistance to RNA degradation (Fig. 1f); for instance, intermediate cloaking (~50% of unpaired 2′-hydroxyls) extended the lifespan of intact eGFP-mRNA by approximately threefold, while extensive cloaking (>90% of accessible 2′-hydroxyls) was capable of further shielding this RNA from thermal cleavage, extending mRNA lifespan by approximately sevenfold (Supplementary Fig. 2). No damage to the nucleobases (for example, deamination of adenine and cytosine) was observed within this time span (Supplementary Fig. 3). Acylation-induced stabilization was further tested on a second, longer mRNA (FLuc-mRNA, Fig. 1g). As before, extensive cloaking (>90% of unpaired 2′-hydroxyls) also almost completely blocked backbone cleavage of Fluc-mRNA over 6 days in water (37 °C).

Diverse acylimidazoles enhance RNA stability in solution

Next, we explored whether the physico-chemical features of acylimidazole reagents can affect their abilities to suppress RNA thermal degradation. We prepared a panel of six additional acylimidazole reagents containing structurally diversified substituents (Fig. 2a). These library reagents were readily prepared with one-step activation of their corresponding low-cost carboxylic acids by 1,1′-carbonyldiimidazole (Extended Data Fig. 2a). In the design of library compounds, we also paid attention to the installation of acyl groups with varied electrophilicity and size, which might later affect the nucleophile-promoted hydrolysis (‘uncloaking’) of acyl adducts to restore RNA. Desired features of acyl adducts include sufficient stability for RNA storage, while being reactive enough to uncloak efficiently. These structural features include aromaticity in **2** and a small acetyl group in **3** that makes acyl adducts more accessible to nucleophiles. We also installed a heteroatom (N or O) at the α-carbon to the carboxyl centre of **4**–**7**, which may promote hydrolysis by electron-withdrawing induction with varied steric bulk. As the maximum level of cloaking varied among **2**–**7**, we proceeded to equimolarly cloak RNA at ~50% of unpaired accessible 2′-hydroxyls of the model RNA to evaluate the effect of different reagents on RNA stability with similar levels of modification (Supplementary Table 1). We also noted that more structured RNA motifs were generally more difficult to cloak (Supplementary Fig. 4). All reagents do not react with the exocyclic amines of nucleobases and 5′-OH of RNA. Most reagents do not react with 3′-OH, except for weak side reactions by **5**–**7** at 3′-OH (Extended Data Fig. 2).

We screened these acylimidazole reagents for modulation of RNA thermal degradation by performing accelerated RNA ageing experiments with eGFP-mRNA aliquots that were equivalently cloaked (~50% of unpaired accessible 2′-OH) with reagents **2**–**7** (Fig. 2b). Representative CE data are shown in Fig. 2c–j for eGFP-mRNA cloaked with **2**–**7**, which resisted thermal degradation across broad substituent types. The smallest (acetylimidazole, **3**) was notable as it attenuated RNA hydrolysis despite lacking a bulky substituent (Fig. 2f). Other alkyl acylimidazoles (**4**–**7**) also greatly augmented the thermal stability of RNA, with ethoxyacetyl compound **6** providing the most stability to eGFP-mRNA (Fig. 2g–j). Noting subtle differences in the stabilization, we hypothesized that the varying protection afforded by the reagents might arise from differential hydrolytic stability of their adducts; this was later confirmed (see below). For example, the slightly reduced enhancement of RNA thermal stability by the *N*,*N*-dimethylglycine (DMG) derivative **4** is likely to be due to faster hydrolysis of the DMG ester at elevated temperatures[29] (Fig. 2g), reflecting possible inductive effects and/or intramolecular general acid facilitation by its protonated tertiary amine[30]. To compensate for this, more extensive cloaking by **4** (>90% of unpaired accessible 2′-OH) extended the lifespan of eGFP-mRNA by approximately fivefold (Fig. 2k). Similarly, cloaking with **4** led to enhanced stability in vitro-transcribed EMX1-single guide RNA (sgRNA) over 9 months when stored at a low temperature (−80 °C) (Supplementary Fig. 5).

Furthermore, a machine learning-based algorithm (DegScore) and in-line sequencing suggested that the ‘hotspots’ of thermal degradation in eGFP-mRNA are located mainly in its unpaired regions (Fig. 2l)[7]. Concomitantly, selective 2′-hydroxyl acylation analysed by primer extension (SHAPE) indicated that the ‘hotspots’ of cloaking by the acylating reagent (for example, **4**) also primarily occur at unpaired sequences of RNA (Fig. 2m). This co-localization of ‘hotspots’ for degradation and cloaking is likely to contribute to the stabilizing effect from 2′-acylation. Taken together, the data confirm that ester adducts of acylimidazoles block RNA thermal degradation. This general stabilizing effect appears to be independent of size and aliphatic versus aromatic construction.

RNA cloaking suppresses enzymatic RNA degradation

High-yield 2′-OH acylation makes it possible to investigate whether 2′-modifications enhance the enzymatic stability of long RNAs (Fig. 3a–f). We systemically surveyed protective effects of cloaking with representative RNases and biofluids, recapitulating the common enzymatic conditions RNAs encounter during storage, handling and application. We found that cloaking with **4** effectively shielded cleavage sites on eGFP-mRNA from nucleolytic degradation by RNase A—the prototypical member of the RNase A superfamily abundant in vertebrate tissues[31–33] and RNase T1—a representative single-stranded RNA (ssRNA)-cleaving endonuclease[34] (Fig. 3c–e). By contrast, other acylating reagents did not sufficiently protect the mRNA against recombinant RNases. We next evaluated whether cloaking could ameliorate mRNA degradation in fetal bovine serum (FBS)[35], a frequent component of eukaryotic cell culture (Fig. 3f). The serum stability of **4**-cloaked eGFP-mRNA is comparable to the stability of liquid nanoparticle-formulated mRNA (Supplementary Fig. 6). This is likely to be due in part to **4** retaining RNA secondary structures and helicity for maximum resistance to RNases (Fig. 2m and Supplementary Fig. 7). Acylating reagents **1, 2, 6** and **7** also protect eGFP-mRNA against FBS to varying degrees. We also showed that cloaking is compatible with formulation with liquid nanoparticles, which together can almost fully shield mRNA from degradation in serum (Supplementary Fig. 6). Thus, 2′-acylation provides context-dependent protection of long RNA (for example, mRNA) against ribonucleolytic enzymes. Reagent **4** effectively shields mRNA against a broad range of RNases.

To explore whether protection against enzymatic degradation by cloaking extends to other biotechnologically relevant RNAs, we systematically characterized how acylimidazoles affect enzymatic degradation of EMX1-sgRNA in serum, a 105 nt sgRNA for CRISPR-Cas9 gene editing (Fig. 3g,h). In general, we found that an increased level of cloaking led to higher serum resistance. Among all reagents, **4** enhanced sgRNA stability the most, by up to 14-fold. Unlike long RNAs, sgRNA was also effectively protected against serum by other acylating reagents with sevenfold to tenfold increases in serum stability. Although such protection is most likely to extend to other RNAs, the secondary structures of RNA may influence the magnitude of enhancement in enzymatic stability (Fig. 3i–k). For example, reagent **4** increases the serum stability of a bulge loop RNA motif and a structurally complex pseudoknot, while having minimal enhancement in serum stability for an internal loop motif. This is likely to be due in part to different RNA motifs having distinct ‘hotspots’ for enzymatic degradation[36,37], which may not be completely shielded by cloaking. Taken together, 2′-acylation effectively enhances the serum stability of RNA, the magnitude of which may be influenced by the length and structure of the underlying RNA.

https://doi.org/10.1038/s41557-023-01246-6

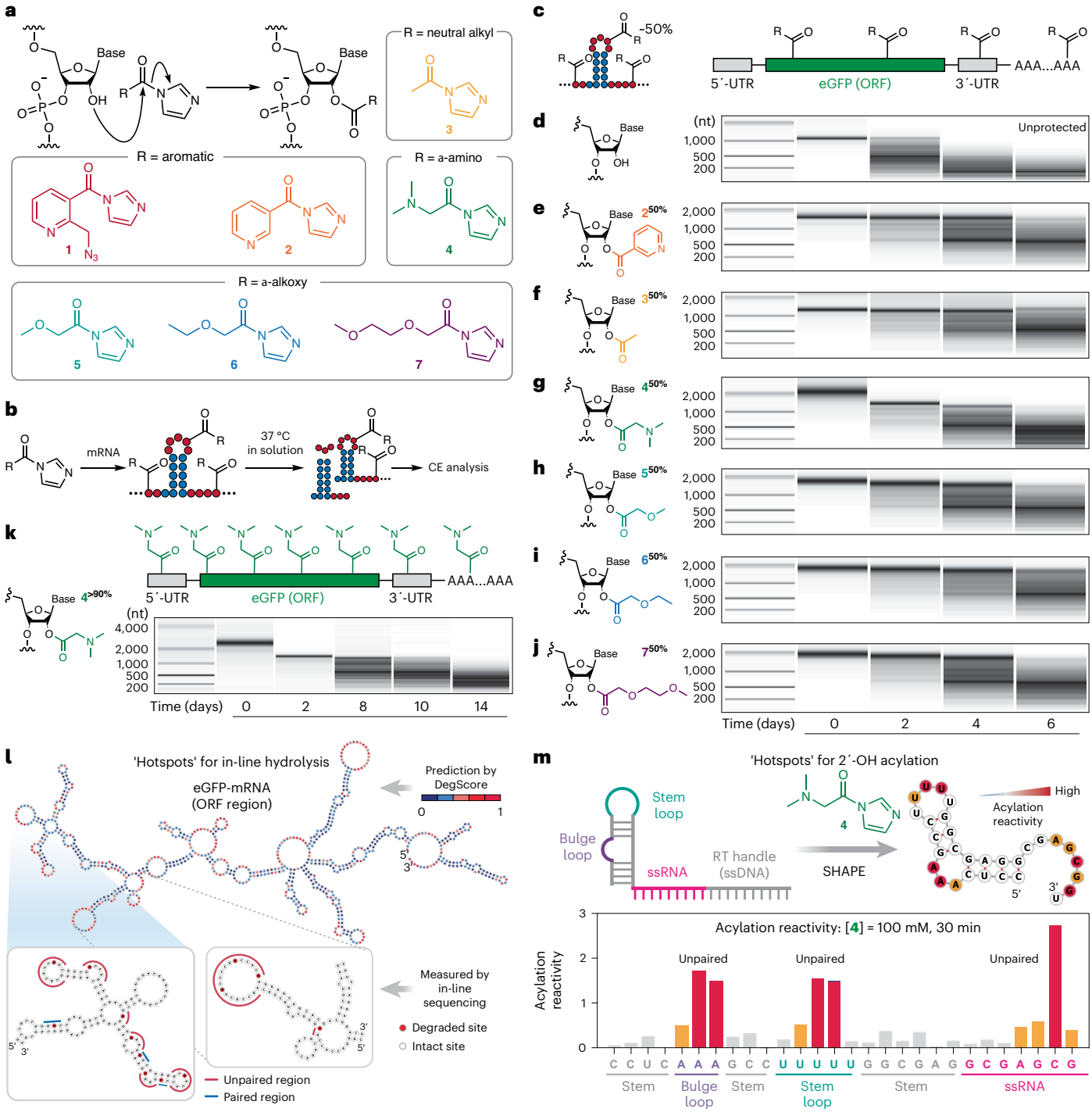

Fig. 2 | Structurally diverse acylimidazole reagents enhance RNA stability in solution. **a**, Structures of acylimidazole agents **1**–**7** clustered by size and electronic properties. **b**, Experimental workflow to determine the thermal stability of cloaked mRNA with CE analysis. **c**–**j**, Qualitative assessment of the apparent RNA quality of unprotected eGFP-mRNA (**d**) or eGFP-mRNA with ~50% of accessible 2′-OH cloaked by **2** (**e**), **3** (**f**), **4** (**g**), **5** (**h**), **6** (**i**) or **7** (**j**) upon incubation in water over time (37 °C). **c**, eGFP-mRNA aliquots were equivalently cloaked (~50% of unpaired accessible 2′-OH) with acylating reagents. Data shown are images of CE traces. The extent of cloaking is annotated as a superscript (**Reagent**$^{\text{cloaking\%}}$). **k**, Stability of eGFP-mRNA with >90% of its 2′-OH cloaked by **4** upon incubation in water over time (37 °C). Note: for **g** and **k**, cloaking reduces the electrophoretic mobility of mRNA in CE. The experiments in **d**–**k** were conducted twice ($n = 2$) with similar results. **l**, 'Hotspots' for in-line hydrolysis of eGFP-mRNA's open reading frame (ORF) determined computationally with the DegScore algorithm (top) and experimentally with in-line sequencing (bottom)[7]. The minimum free energy structure of mRNA was calculated using Vienna RNAfold[51]. Top: the colour of each nucleotide corresponds to its propensity for hydrolysis based on the calculated DegScore (0 to 1.0) as illustrated. Bottom: sites for degradation are coloured red. **m**, 'Hotspots' for 2′-OH acylation by **4** are located in the unpaired regions of RNA determined using SHAPE analysis. Nucleotides that are highly, intermediately and minimally susceptible for 2′-OH acylation are coloured red, yellow and white, respectively.

https://doi.org/10.1038/s41557-023-01246-6

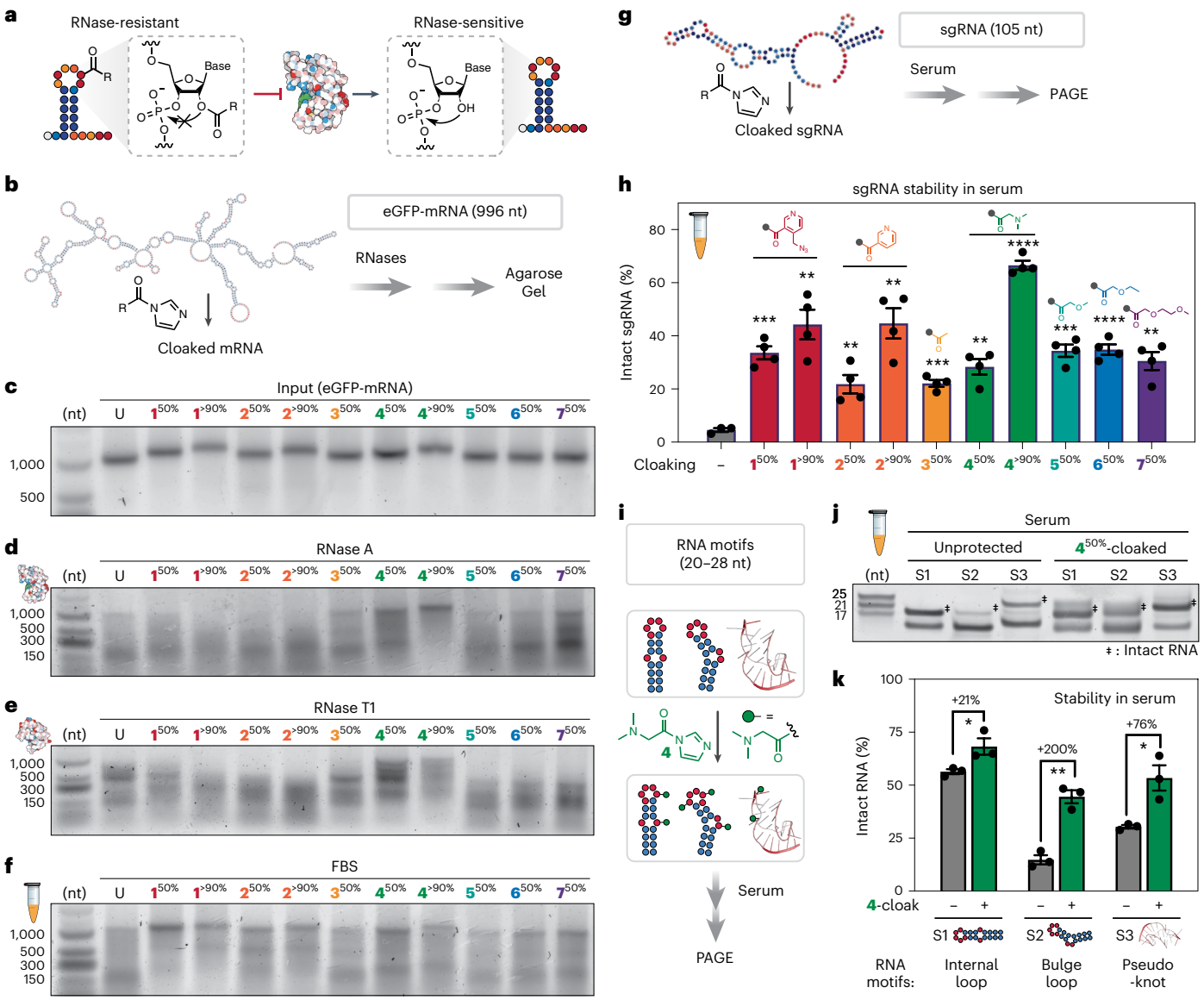

Fig. 3 | RNA cloaking suppresses enzymatic RNA degradation by RNases and biofluids. a, RNA cloaking confers resistance to degradation by RNases. **b**, Experimental workflow to quantify RNA integrity of eGFP-mRNA after treatment with RNA-degrading enzymes and biofluids. **c**, Representative agarose gel showing the integrity of eGFP-mRNA that was cloaked with different acylating reagents at various levels of cloaking. **d**–**f**, Representative agarose gel showing the impacts of acylating reagents and level of cloaking on eGFP-mRNA degradation by RNase A (**d**), RNase T1 (**e**) and FBS (**f**) in vitro. The experiments were conducted three times with similar results. **g**, Experimental workflow to evaluate the resistance of cloaked 105 nt EMX1-sgRNA against serum degradation. **h**, Plot comparing the integrity of the EMX1-sgRNA after treatment with FBS. RNA is unprotected or cloaked with **1**–**7**. Data represent mean ± s.e.m., $n = 3$ (unmodified RNA) and $n = 4$ (cloaked RNA) independent experiments. **i**, Experimental workflow to evaluate the stability of diverse **4**-cloaked RNA structural motifs in serum. **j**–**k**, Representative PAGE gel (**j**) and plot (**k**) showing the impacts of RNA structure on serum stability. For **k**, data represent mean ± s.e.m., $n = 3$ independent experiments. Statistical significance was calculated with two-tailed unpaired *t*-tests: $^{*}P < 0.05$, $^{**}P < 0.01$, $^{***}P < 0.001$, $^{****}P < 0.0001$. For **h**, *P* values are 0.0002 (**1**$^{50\%}$), 0.0019 (**1**$^{>90\%}$), 0.0087 (**2**$^{50\%}$), 0.0019 (**2**$^{>90\%}$), 0.0001 (**3**$^{50\%}$), 0.0011 (**4**$^{50\%}$), < 0.0001 (**4**$^{>90\%}$), 0.0001 (**5**$^{50\%}$), <0.0001 (**6**$^{50\%}$) and 0.0014 (**7**$^{50\%}$). For **k**, *P* values are 0.0413 (S1), 0.0014 (S2) and 0.0185 (S3).

Nucleophiles remove 2′-polyacylation to uncloak RNA

Nucleophiles are known to catalyse ester hydrolysis; examples include the use of imidazole and pyridine as nucleophilic catalysts[38]. To restore biological activity of RNAs after cloaking-based stabilization, we tested uncloaking strategies to promote rapid hydrolysis of 2′-carboxyl esters with weakly basic nucleophiles (Fig. 4a). To this end, we assembled a panel of 13 reagents that were known as strong nucleophiles or promoters of ester hydrolysis[39], with pK_a values ranging from −10 to 9.7 (Fig. 4b). In the library design, we avoided the use of strong Brønsted bases to prevent hydrolytic RNA backbone cleavage[40]. Nucleophiles were screened against the 18 nt model RNA containing acyl groups of each type at 37 °C and neutral pH. This identified at least nine sensitive acylation-nucleophile pairs that promoted >50% removal of adducts within 2 h (Fig. 4c and Extended Data Fig. 3). Among these, acyl adducts from **1** can be reversed via a Staudinger reaction[24], although we previously found this reversal strategy cannot be readily adapted for long RNA (>600 nt)[41]. Adducts from **4**–**7** can also be rapidly removed with designated nucleophiles, with half-lives for reversal ranging from 1.1 to 1.8 h (Fig. 4d). Adducts from **2**–**3** are relatively resistant to reversal by non-basic nucleophiles and were not pursued further.

The sensitivities of 2′-acyl adducts towards each nucleophile correlate with their physico-chemical properties (Fig. 4c). Aliphatic adducts showed distinct sensitivities towards library nucleophiles. For the 2′-acyl adduct from **4**, the effects of the biocompatible

https://doi.org/10.1038/s41557-023-01246-6

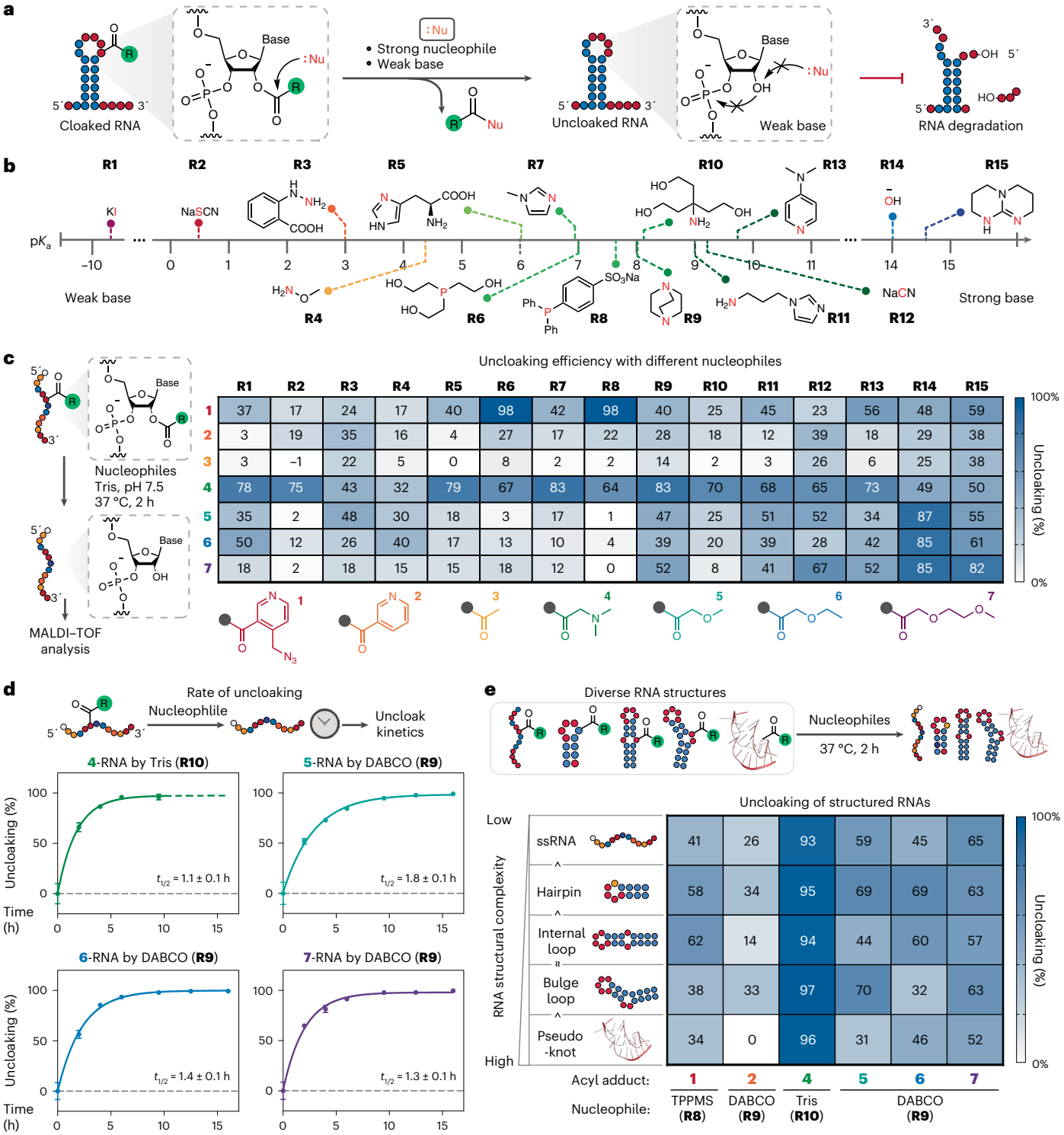

	R1	R2	R3	R4	R5	R6	R7	R8	R9	R10	R11	R12	R13	R14	R15
1	37	17	24	17	40	98	42	98	40	25	45	23	56	48	59
2	3	19	35	16	4	27	17	22	28	18	12	39	18	29	38
3	3	–1	22	5	0	8	2	2	14	2	3	26	6	25	38
4	78	75	43	32	79	67	83	64	83	70	68	65	73	49	50
5	35	2	48	30	18	3	17	1	47	25	51	52	34	87	55
6	50	12	26	40	17	13	10	4	39	20	39	28	42	85	61
7	18	2	18	15	15	18	12	0	52	8	41	67	52	85	82

	ssRNA	Hairpin	Internal loop	Bulge loop	Pseudo -knot
1 (TPPMS (R8))	41	58	62	38	34
2 (DABCO (R9))	26	34	14	33	0
4 (Tris (R10))	93	95	94	97	96
5 (DABCO (R9))	59	69	44	70	31
6 (DABCO (R9))	45	69	60	32	46
7 (DABCO (R9))	65	63	57	63	52

Fig. 4 | Nucleophilic reagents remove 2′-polyacylation to uncloak RNA. **a**, General strategy for non-basic nucleophiles promoting RNA uncloaking. **b**, Chemical structures of 15 non-basic nucleophilic reagents (**R1**–**R15**) ranked by the pK_a of their conjugate acids (electrophilic centres highlighted in orange). **c**, Experimental workflow to screen nucleophiles for RNA uncloaking with an 18 nt model RNA. MALDI–TOF analysis quantifies the efficiency of 2′-ester hydrolysis. Heat map comparing the levels of uncloaking by various non-basic nucleophiles at pH 7.5 after 2 h at 37 °C. Phosphines (**R6** and **R8**) reverse 2′-acylation by **1** at 1 mM via Staudinger reduction[24]. Other tests were performed with 50 mM of nucleophiles. **d**, Quantitative assessment of the apparent hydrolytic rate of 2′-acyl adducts from **4** in Tris buffer and **5**–**7** in DABCO-containing solution at pH 7.5 (50 mM, 37 °C), as measured by MALDI–TOF. Half-lives were calculated via non-linear regression (one-phase decay model). Data represent mean ± s.e.m., $n = 3$ independent experiments. The dashed curve in green was extrapolated. **e**, Heat map comparing the hydrolysis of 2′-carboxyl esters on diverse RNA structural motifs by nucleophiles at pH 7.5 (50 mM, 2 h, 37 °C). In **c** and **e**, the numbers in the heat map represent percentage reversal of 2′-acyl adducts per RNA at 2 h.

https://doi.org/10.1038/s41557-023-01246-6

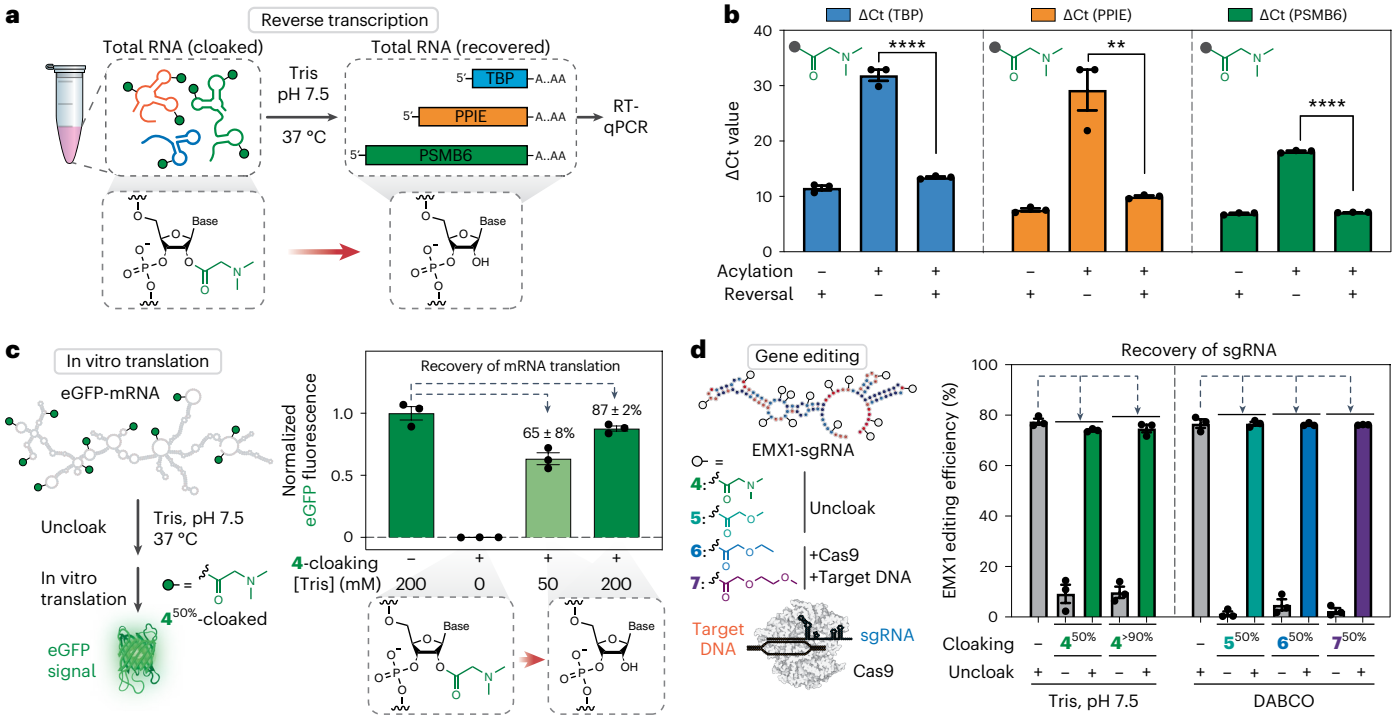

Fig. 5 | Nucleophile-promoted RNA uncloaking restores RNA functions. **a**, Experimental workflow to restore reversible transcription of **4**-cloaked cellular mRNA with Tris buffer alone. **b**, Bar graph comparing the ΔCt values for three representative isolated cellular mRNA before and after uncloaking by Tris. **c**, Experimental workflow to restore translation of **4**-cloaked (50 or 90%) eGFP-mRNA with Tris (left) and bar graphs comparing eGFP expression before and after uncloaking by Tris (right). **d**, Left: experimental workflow to recover gene-editing function of **4**-cloaked (50 or 90%) by 200 mM of Tris and **5**-/**6**-/**7**-cloaked (50%) EMX1-sgRNA by 50 mM DABCO. Right: bar graph comparing the efficiency of EMX1-sgRNA-mediated double-stranded DNA cleavage before and after uncloaking. Note: the reaction buffer contains Tris, which leads to ~10% basal level of DNA cleavage. In **b**, **c** and **d**, data represent mean ± s.e.m., $n = 3$ independent experiments. Statistical significance was calculated with two-tailed unpaired Student's t-tests: $^{*}P < 0.05$, $^{**}P < 0.01$, $^{***}P < 0.001$, $^{****}P < 0.0001$. For **b**, P values are <0.0001 (TBP), 0.0063 (PPIE) and <0.0001 (PSMB6).

tris(hydroxymethyl)aminomethane (Tris) buffer alone were substantial, consistent with previous reports that Tris can hydrolyse active esters[42,43]. Interestingly, and in contrast, the simple acetyl adducts from acetylimidazole (**3**) were not reversed by Tris, nor by any of the other conditions tested. This suggests that the electron-withdrawing heteroatom at the α-carbon of DMG-derivative **4** sensitizes the ester for hydrolysis. Notably, alkoxyesters of **5**–**7** displayed major differences in their vulnerabilities towards nucleophiles compared to the DMG ester, further showing that substituents at the α-carbon can significantly modulate an ester's susceptibility towards nucleophiles.

Moreover, permutations and combinations of seven reagents (**1**–**7**) with five RNA structural motifs demonstrate that cloaking may also correlate with the underlying RNA structure (Fig. 4e). Uncloaking by phosphine (**R8**) and 1,4-diazabicyclo[2.2.2]octane (DABCO) (**R9**) is substantially influenced by RNA structure, wherein more structured RNAs (for example, pseudoknot) appear to be more difficult to uncloak by phosphine and DABCO. This is likely to be due to their reduced accessibility to bulky nucleophiles. By contrast, Tris potently uncloaks DMG adducts of **4** regardless of the underlying RNA structure, making **4**/Tris a cloaking/uncloaking pair suitable for protection of long RNAs with intricate folding.

Nucleophiles uncloak RNA to restore RNA functions

Although our nucleophilic reagents could restore a relatively short RNA, a practical challenge remained; namely, whether these reagents could be employed to recover much longer and more sensitive RNAs while keeping the strands intact and functional. For instance, the ability of a single 2′-acylation to halt reverse transcriptase during primer extension necessitates efficient 2′-deacylation to avoid premature reverse transcription termination[21]. Considering that **4** can maximally protect long RNAs against a broad range of RNases and demonstrates the fastest reversal kinetics (Fig. 3d–f and Fig. 4d), we assessed whether these nucleophiles could restore reverse transcription of **4**-cloaked RNA (Fig. 5a). We isolated and cloaked total cellular RNA from HEK293 cells with reagent **4** and recovery efficiency was evaluated for three representative mRNAs by the reverse transcription efficiencies. Quantitative PCR with reverse transcription (RT-qPCR) results in Fig. 5a,b showed that incubation with Tris alone at neutral pH reinstated the reverse transcription of the cloaked mRNAs (TBP, PPIE and PSMB6) after 24 h, regardless of their transcript and amplicon lengths. Additionally, the restored cellular RNA can remain largely intact (Supplementary Fig. 8) and demonstrated similar or the same ΔCt values (ΔCt = Ct (gene of interest) − Ct (reference gene); Ct, cycle threshold) compared to their unprotected counterparts, establishing that RNA uncloaking by Tris is biocompatible for effective recovery of reverse transcription of diverse RNAs.

Recent experiments have shown that local 2′-acylation can terminate translation when introduced into the coding region of mRNAs (refs. 41,44). Thus, we investigated whether Tris could restore the translation of a model eGFP-mRNA densely cloaked (50%) by **4**. Based on in vitro translation assays, cloaking with **4** strongly blocked the translation of eGFP-mRNA, while treatment with Tris (pH 7.5) at 37 °C rendered up to 87% restoration of eGFP expression (Fig. 5c). Electrophoresis experiments showed that the mRNA integrity remained largely unchanged after uncloaking (Supplementary Fig. 9). These data suggested that Tris alone can recover mRNA translation of adducts of **4**, while keeping the RNA intact. To explore the generality of this observation, we applied the methods to an in vitro transcribed CRISPR

https://doi.org/10.1038/s41557-023-01246-6

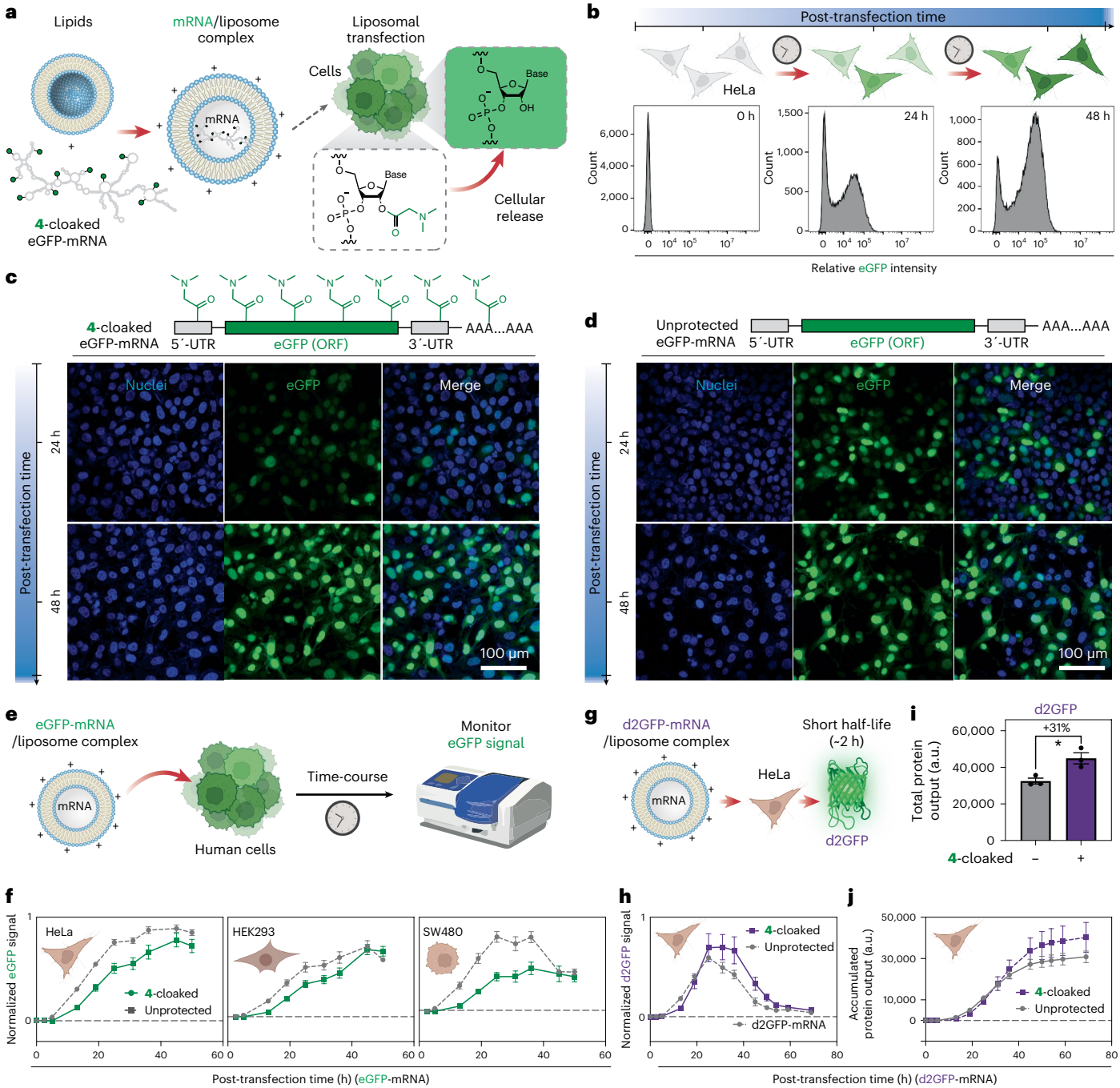

Fig. 6 | Spontaneous RNA uncloaking restores mRNA translation with extended functional half-lives in human cells. a, General schematic for liposomal delivery of cloaked mRNA to spontaneously release mRNA and restore translation in cells. **b**, Fluorescence-activated cell sorting analysis determines eGFP expression of HeLa cells transfected with **4**-cloaked eGFP-RNA over 2 days. **c**,**d**, Representative single-blind fluorescence micrographs of HeLa cells transfected with **4**-cloaked eGFP-mRNA (**c**) and unprotected eGFP-mRNA (**d**) at 24 and 48 h. Each condition was imaged at areas that contain more than 50 cells over two independent experiments. The cell images are representative fluorescence images showing distribution of expression levels of eGFP. **e**, Schematic for a fluorimeter-based assay to measure the kinetics of eGFP-mRNA translation. **f**, **4**-Cloaked eGFP-mRNA translates in HeLa (left), HEK293 (middle) and SW480 (right) cells. **g**, Liposomal transfection of d2GFP-mRNA into HeLa cells. **h**, Cloaking by **4** extended the translation of d2GFP-mRNA in HeLa cells. **i**, Cloaking by **4** enhanced the total protein output of d2GFP-mRNA after 69 h. a.u., arbitrary unit. **j**, Accumulated protein output of d2GFP-mRNA with or without cloaking by **4** at indicated time points. In **f** and **h**–**j**, data represent mean ± s.e.m., $n = 3$ biologically independent experiments. Cell illustrations in **a**, **b** and **e** created with Biorender.com.

sgRNA (refs. 14,25) (Fig. 5d). Acylation of EMX1-sgRNA by **4**–**7** blocked its cleavage function (<10%) in vitro. Treatment of cloaked sgRNA with Tris (for **4**-cloaked sgRNA) or DABCO (for **5**-/**6**-/**7**-cloaked sgRNA) at neutral pH for 11 h fully restored DNA cleavage, while sgRNA remained largely undegraded (Supplementary Fig. 10).

Spontaneous uncloaking in cells restores mRNA translation

Intact cells maintain high intracellular concentrations of nucleophilic species such as cysteine and glutathione. The sensitivity observed here of 2′-carboxyl esters towards nucleophilic hydrolysis suggests the possibility of spontaneous RNA uncloaking both during and after

cellular delivery, which might enable RNA functional recovery (Fig. 6a). To explore this possibility, we employed cloaked mRNAs encoding fluorescent reporter proteins. Indeed, we observed the emergence of strong green fluorescence signals by flow cytometry over a period of 2 days in HeLa cells transfected with intermediately **4**-cloaked eGFP-mRNA (Fig. 6b). Single-blind fluorescence imaging further confirmed that the translation of **4**-cloaked eGFP-mRNA was restored after an initial delay compared to its unprotected counterpart (Fig. 6c,d), corroborating the spontaneous RNA uncloaking in live cells. In marked contrast, for eGFP-mRNA that was cloaked with **1**, translation remained strongly inhibited (Extended Data Fig. 4a). This further confirmed that the recovery of eGFP expression is due to the releasing properties of the DMG ester of **4**. Testing in two additional cell lines (SW480, HEK293) confirmed generality (Fig. 6e,f). Moreover, the delayed translation of cloaked mRNAs reflects an initial uncloaking step, which when occurring over time may provide slow-release translation kinetics—reducing an early expression peak and extending the duration of translation (see below). Finally, we also observed that translation of eGFP-mRNA with α-alkoxyl acyl adduct **7** can also be restored in cells, highlighting possible control over mRNA release kinetics by modification of the acyl group (Extended Data Fig. 4b).

We next investigated how cloaking affects the functional lifespan of mRNA in cells. As eGFP protein is highly stable with a half-life >24 h (ref. 45), protein degradation alone dominates expression and provides no information about mRNA functional half-lives[46]. We therefore adopted a reporter system employing mRNA encoding a destabilized green fluorescent protein d2GFP, where both mRNA and protein degradation occur with similar half-lives of ~2–3 h (Fig. 6g)[46,47]. We observed that the translation of unprotected d2GFP-mRNA quickly descended after peaking (Fig. 6h). By contrast, intermediate cloaking by **4** led to sustained d2GFP-mRNA translation at its peak level for ~10 h, strongly suggesting its ability to extend the functional lifespan of d2GFP-mRNA effectively. This extended mRNA functional half-life also enhanced the total protein output of d2GFP-mRNA by 31% in HeLa cells (Fig. 6i) and this enhancement became increasingly prominent after ~31 h post-transfection compared to unprotected d2GFP-mRNA (Fig. 6j). Taken together, RNA cloaking by DMG derivative **4** effectively extended the d2GFP-mRNA functional lifespan and translation, providing insights for the potential use of reversible 2′-acylation as a modulator of mRNA translation kinetics.

Conclusions

We have shown that RNA cloaking by reversible 2′-hydroxyl acylation effectively enhances the thermal and nucleolytic stability of a wide range of RNAs. No previous studies have systematically explored how reversible 2′-modification affects RNA thermal and enzymatic stabilities, especially for long RNAs. The high-yield cloaking by water-soluble acylimidazoles can be broadly applied in one step to RNA of any origin, making it a remarkably simple and general strategy for preservation of the biopolymer. We note that the marked enhancement of RNA half-lives presents strong implications for improved RNA storage and could ease the need for costly ultracold conditions. Further increases in RNA half-lives through cloaking are likely to be possible, as resistance towards thermal degradation depends on the hydrolytic stability of 2′-acyl adducts, which can be tuned. Furthermore, cell-permeable acylimidazoles can acylate RNA in tissues[21], suggesting the future utility of these features during RNA isolation for biomolecular or clinical studies.

To restore biological activity after storage, efficient unblocking of RNAs is necessary. We have shown that water-soluble nucleophiles can reverse 2′-acylation to restore numerous RNA functions. We find that 2′-α-alkoxyesters are sensitive to multiple nucleophiles and the DMG-ester adducts of **4** are especially sensitive to nucleophiles including Tris buffer (pH 7.5). Notably, other buffers lacking the primary amine of Tris such as MOPS and HEPES, or other primary amine-containing nucleophiles, do not significantly facilitate hydrolysis of the DMG ester at physiological pH (Supplementary Fig. 11). These data suggest the unique structure of Tris may preferentially promote DMG-ester hydrolysis[38,42,43]. Additional mechanistic studies with relevant nucleophile analogues will be useful in exploring this hypothesis in the future.

Our kinetics studies provide evidence regarding the application of RNA cloaking for extended release of RNA functions in cells. We find that the translation of **4**-cloaked eGFP-mRNA was initiated after an ~7 h delay compared to its unprotected counterpart, which reflects the existence of the deacylation processes. Our preliminary data suggest that three types of biochemical including transfection reagent (lipofectamine)[48,49], culturing medium and a mixture of free amino acids, together with other components in the mammalian cells, appear to accelerate uncloaking in the context of mRNA delivery (Supplementary Fig. 12). Another useful feature of RNA cloaking is the ability to increase mRNA functional half-lives in cells. We have shown that cloaking by **4** extended the peak d2GFP-mRNA translation by ~10 h, which is >3-fold of the reported half-life of unmodified d2GFP-mRNA (3 h)[50] and enabled greater overall protein expression. Understanding this phenomenon will provide mechanistic insights into future efforts to leverage 2′-modifications for modulating RNA pharmacokinetics. Systematic studies of reverse 2′-acylation for modulating mRNA translation are currently underway.

Online content

Any methods, additional references, Nature Portfolio reporting summaries, source data, extended data, supplementary information, acknowledgements, peer review information; details of author contributions and competing interests; and statements of data and code availability are available at https://doi.org/10.1038/s41557-023-01246-6.

References

1. Fabre, A. L., Colotte, M., Luis, A., Tuffet, S. & Bonnet, J. An efficient method for long-term room temperature storage of RNA. *Eur. J. Hum. Genet.* **22**, 379–385 (2014).
2. Wayment-Steele, H. K. et al. Theoretical basis for stabilizing messenger RNA through secondary structure design. *Nucleic Acids Res.* **49**, 10604–10617 (2021).
3. Kellerman, D. L., York, D. M., Piccirilli, J. A. & Harris, M. E. Altered (transition) states: mechanisms of solution and enzyme catalyzed RNA 2′-*O*-transphosphorylation. *Curr. Opin. Chem. Biol.* **21**, 96–102 (2014).
4. Guo, F. et al. Effect of ribose conformation on RNA cleavage via internal transesterification. *J. Am. Chem. Soc.* **140**, 11893–11897 (2018).
5. Breslow, R. & Chapman, W. H. Jr On the mechanism of action of ribonuclease A: relevance of enzymatic studies with a p-nitrophenylphosphate ester and a thiophosphate ester. *Proc. Natl Acad. Sci. USA* **93**, 10018–10021 (1996).
6. Lee, J. B., Hong, J., Bonner, D. K., Poon, Z. & Hammond, P. T. Self-assembled RNA interference microsponges for efficient siRNA delivery. *Nat. Mater.* **11**, 316–322 (2012).
7. Leppek, K. et al. Combinatorial optimization of mRNA structure, stability, and translation for RNA-based therapeutics. *Nat. Commun.* **13**, 1536 (2022).
8. Hendel, A. et al. Chemically modified guide RNAs enhance CRISPR-Cas genome editing in human primary cells. *Nat. Biotechnol.* **33**, 985–989 (2015).
9. Miller, P. S. et al. Nonionic nucleic acid analogues. Synthesis and characterization of dideoxyribonucleoside methylphosphonates. *Biochemistry* **18**, 5134–5143 (1979).
10. Wu, S. Y. et al. 2′-OMe-phosphorodithioate-modified siRNAs show increased loading into the RISC complex and enhanced anti-tumour activity. *Nat. Commun.* **5**, 3459 (2014).

11. Korobeynikov, V. A., Lyashchenko, A. K., Blanco-Redondo, B., Jafar-Nejad, P. & Shneider, N. A. Antisense oligonucleotide silencing of FUS expression as a therapeutic approach in amyotrophic lateral sclerosis. *Nat. Med.* **28**, 104–116 (2022).
12. Yin, H. et al. Structure-guided chemical modification of guide RNA enables potent non-viral in vivo genome editing. *Nat. Biotechnol.* **35**, 1179–1187 (2017).
13. Guinea-Viniegra, J. et al. Targeting miR-21 to treat psoriasis. *Sci. Transl. Med.* **6**, 225re221 (2014).
14. Wang, S. R. et al. Conditional control of RNA-guided nucleic acid cleavage and gene editing. *Nat. Commun.* **11**, 91 (2020).
15. Ovodov, S. & Alakhov, Yu,B. mRNA acetylated at 2′-OH-groups of ribose residues is functionally active in the cell-free translation system from wheat embryos. *FEBS Lett.* **270**, 111–114 (1990).
16. Goldsborough, S. Modified polynucleotides and uses thereof. US patent 2003/0039985 A1 (2003).
17. Steen, K. A., Siegfried, N. A. & Weeks, K. M. Selective 2′-hydroxyl acylation analyzed by protection from exoribonuclease (RNase-detected SHAPE) for direct analysis of covalent adducts and of nucleotide flexibility in RNA. *Nat. Protoc.* **6**, 1683–1694 (2011).
18. Fessler, A. B. et al. Water-soluble isatoic anhydrides: a platform for RNA-SHAPE analysis and protein bioconjugation. *Bioconjug. Chem.* **29**, 3196–3202 (2018).
19. Fessler, A. B., Fowler, A. J. & Ogle, C. A. Directly quantifiable biotinylation using a water-soluble isatoic anhydride platform. *Bioconjug. Chem.* **32**, 904–908 (2021).
20. Velema, W. A. & Kool, E. T. The chemistry and applications of RNA 2′-OH acylation. *Nat. Rev. Chem.* **4**, 22–37 (2020).
21. Spitale, R. C. et al. Structural imprints in vivo decode RNA regulatory mechanisms. *Nature* **519**, 486–490 (2015).
22. Velema, W. A., Kietrys, A. M. & Kool, E. T. RNA control by photoreversible acylation. *J. Am. Chem. Soc.* **140**, 3491–3495 (2018).
23. Park, H. S., Kietrys, A. M. & Kool, E. T. Simple alkanoyl acylating agents for reversible RNA functionalization and control. *Chem. Commun.* **55**, 5135–5138 (2019).
24. Kadina, A., Kietrys, A. M. & Kool, E. T. RNA cloaking by reversible acylation. *Angew. Chem. Int. Ed. Engl.* **57**, 3059–3063 (2018).
25. Habibian, M. et al. Reversible RNA acylation for control of CRISPR-Cas9 gene editing. *Chem. Sci.* **11**, 1011–1016 (2019).
26. Li, Y. & Breaker, R. R. Kinetics of RNA degradation by specific base catalysis of transesterification involving the 2′-hydroxyl group. *J. Am. Chem. Soc.* **121**, 5364–5372 (1999).
27. Soukup, G. A. & Breaker, R. R. Relationship between internucleotide linkage geometry and the stability of RNA. *RNA* **5**, 1308–1325 (1999).
28. Duffy, K., Arangundy-Franklin, S. & Holliger, P. Modified nucleic acids: replication, evolution, and next-generation therapeutics. *BMC Biol.* **18**, 112 (2020).
29. Takata, J. et al. Vitamin K prodrugs: 1. Synthesis of amino acid esters of menahydroquinone-4 and enzymatic reconversion to an active form. *Pharm. Res.* **12**, 18–23 (1995).
30. Johnson, S. L. in *Advances in Physical Organic Chemistry* Vol. 5 (ed. Gold, V.) 237–330 (Academic Press, 1967).
31. delCardayre, S. B. & Raines, R. T. Structural determinants of enzymatic processivity. *Biochemistry* **33**, 6031–6037 (1994).
32. Raines, R. T. Ribonuclease A. *Chem. Rev.* **98**, 1045–1066 (1998).
33. Garnett, E. R. & Raines, R. T. Emerging biological functions of ribonuclease 1 and angiogenin. *Crit. Rev. Biochem. Mol. Biol.* **57**, 244–260 (2022).
34. Pace, C. N., Heinemann, U., Hahn, U. & Saenger, W. Ribonuclease T1: structure, function, and stability. *Angew. Chem. Int. Ed. Engl.* **30**, 343–360 (1991).
35. Tsui, N. B., Ng, E. K. & Lo, Y. M. Stability of endogenous and added RNA in blood specimens, serum, and plasma. *Clin. Chem.* **48**, 1647–1653 (2002).
36. Daou-Chabo, R. & Condon, C. RNase J1 endonuclease activity as a probe of RNA secondary structure. *RNA* **15**, 1417–1425 (2009).
37. Wang, Z., Treder, K. & Miller, W. A. Structure of a viral cap-independent translation element that functions via high affinity binding to the eIF4E subunit of eIF4F. *J. Biol. Chem.* **284**, 14189–14202 (2009).
38. Jencks, W. P. & Carriuolo, J. Reactivity of nucleophilic reagents toward esters. *J. Am. Chem. Soc.* **82**, 1778–1786 (1960).
39. van der Helm, M. P., Klemm, B. & Eelkema, R. Organocatalysis in aqueous media. *Nat. Rev. Chem.* **3**, 491–508 (2019).
40. Jarvinen, P., Oivanen, M. & Lonnberg, H. Interconversion and phosphoester hydrolysis of 2′,5′- and 3′,5′-dinucleoside monophosphates: kinetics and mechanisms. *J. Org. Chem.* **56**, 5396–5401 (1991).
41. Xiao, L., Jun, Y. W. & Kool, E. T. DNA tiling enables precise acylation-based labeling and control of mRNA. *Angew. Chem. Int. Ed. Engl.* **60**, 26798–26805 (2021).
42. Werber, M. M. & Shalitin, Y. The reaction of tertiary amino alcohols with active esters: I. Acylation and deacylation steps. *Bioorg. Chem.* **2**, 202–220 (1973).
43. de Jersey, J., Fihelly, A. K. & Zerner, B. On the mechanism of the reaction of tris(hydroxymethyl)aminomethane with activated carbonyl compounds: a model for the serine proteinases. *Bioorg. Chem.* **9**, 153–162 (1980).
44. Park, H. S., Jash, B., Xiao, L., Jun, Y. W. & Kool, E. T. Control of RNA with quinone methide reversible acylating reagents. *Org. Biomol. Chem.* **19**, 8367–8376 (2021).
45. Kain, S. R. Green fluorescent protein (GFP): applications in cell-based assays for drug discovery. *Drug Discov. Today* **4**, 304–312 (1999).
46. Singh, A., Razooky, B. S., Dar, R. D. & Weinberger, L. S. Dynamics of protein noise can distinguish between alternate sources of gene-expression variability. *Mol. Syst. Biol.* **8**, 607 (2012).
47. Li, X. et al. Generation of destabilized green fluorescent protein as a transcription reporter. *J. Biol. Chem.* **273**, 34970–34975 (1998).
48. LoPachin, R. M. & Gavin, T. Reactions of electrophiles with nucleophilic thiolate sites: relevance to pathophysiological mechanisms and remediation. *Free Radic. Res.* **50**, 195–205 (2016).
49. Hou, X., Zaks, T., Langer, R. & Dong, Y. Lipid nanoparticles for mRNA delivery. *Nat. Rev. Mater.* **6**, 1078–1094 (2021).
50. Raj, A., Peskin, C. S., Tranchina, D., Vargas, D. Y. & Tyagi, S. Stochastic mRNA synthesis in mammalian cells. *PLoS Biol.* **4**, e309 (2006).
51. Kerpedjiev, P., Hammer, S. & Hofacker, I. L. Forna (force-directed RNA): simple and effective online RNA secondary structure diagrams. *Bioinformatics* **31**, 3377–3379 (2015).

Methods

Materials

DNA and RNA were purchased from IDT, TriLink BioTechnology or Stanford PAN facility unless otherwise stated (see Supplementary Table 2 for details). All chemicals purchased from commercial suppliers were used without further purification (see Supplementary Table 3 for details). All enzymes, kits, bioreagents and software were obtained from the sources listed in Supplementary Table 3. Human cell lines HEK293 (CRL-1573), HeLa (CRM-CCL-2) and SW480 (CCL-228) were purchased from American Type Culture Collection and maintained in Dulbecco's modified Eagle medium (DMEM) supplemented with 10% FBS at 37 °C in a humidified incubator containing 5% CO_2.

Synthesis of acylimidazole reagents (1-7)

Reagent **1** was synthesized according to previously reported protocols[21]. Reagents **2**–**7** were synthesized with the following general protocol. The carboxylic acid precursor (1.0 equiv.) was dissolved in dry dimethylsulfoxide (DMSO) as a 4 M solution. To it was added an equal volume of a suspension containing 1.0 equiv. 1,1′-carbonyldiimidazole at room temperature. The resulting solution was stirred at room temperature for 4 h. After the reaction, the crude solution can be stored and used as a 2 M acylimidazole stock solution without further purification. The final solution is a 1:1 mixture of an acylimidazole and free imidazole, verified by ^{1}H NMR spectroscopy, ^{13}C NMR spectroscopy and high-resolution mass spectrometry (HRMS) (see Supplementary Information for detailed compound-specific synthetic protocols).

In vitro transcription

The template for in vitro transcription (IVT) of EMX1-sgRNA was generated according to previously reported protocols[52]. EMX1-sgRNA was then synthesized through IVT with the HiScribe T7 High Yield RNA Synthesis Kit (NEB, E2040S) according to the manufacturer's protocol. The IVT template of d2GFP-mRNA was cloned according to previously reported protocols[53]. Then d2GFP-mRNA was generated through IVT with the HiScribe T7 High Yield RNA Synthesis Kit according to the manufacturer's protocol. The resulting mRNA was capped with the Vaccinia Capping System according to the manufacturer's protocol. See Supplementary Table 2 for related oligonucleotide sequences.

RNA purification by ethanol precipitation

The reaction solution was diluted to 100 µl with RNase-free water. Then 10 µl of 3 M NaOAc (pH 5.5) and 1 µl of RNA-grade glycogen (20 µg µl^{-1}) were added and the mixture was vortexed. Next, 500 µl of ice-cold 96% ethanol was added and the mixture was vortexed. The resulting mixture was incubated at −80 °C overnight and then centrifuged at 21,100*g* for 40 min to form a pellet. The pellet was washed with 200 µl ice-cold 70% ethanol once and air-dried for 15 min. RNA was reconstituted with RNase-free water.

RNA cloaking

The cloaked RNAs were generated by reacting RNAs with acylimidazole reagents in aqueous solutions. After cloaking, short RNAs (tRF-3005 RNA and IR700-RNA) were purified by precipitation with ethanol as described above. The other RNAs (EMX1-sgRNA, eGFP-mRNA, d2GFP-mRNA, Fluc-mRNA and total cellular RNA) were purified with RNA Cleanup & Concentrator Column-5 according to the manufacturer's protocol. Note: to acylate RNA with modified nucleobases that contain relatively potent nucleophiles (for example, queuosine), the nucleobases' resistance to acylation may need to be evaluated for undisrupted RNA functions after uncloaking.

To generate intermediately (~50%) **1**-cloaked RNA, 500 ng of RNA (tRF-3005 RNA, IR700-RNA, EMX1-sgRNA or eGFP-mRNA) was diluted to an 8 µl solution with RNase-free water. Then 2 µl of 750 mM stock of **1** in DMSO was added to the RNA solution. The reaction mixture was then incubated at room temperature for 4 h. To generate extensively (>90%) **1**-cloaked RNA, 500 ng of RNA (tRF-3005 RNA, IR700-RNA, EMX1-sgRNA, eGFP-mRNA or Fluc-mRNA) was diluted to an 8 µl solution with RNase-free water. Then 2 µl of 1.5 M stock of **1** in DMSO was added to the RNA solution. The mixture was incubated at 37 °C for 4 h.

To generate intermediately (~50%) **2**-cloaked RNA, 500 ng of RNA (tRF-3005 RNA or eGFP-mRNA) was diluted to an 8 µl solution with RNase-free water. Then 2 µl of 1 M stock of 2 in DMSO was added to the RNA solution. The mixture was incubated at room temperature for 4 h. To generate extensively (>90%) **1**-cloaked RNA, 2.5 µg of RNA (EMX1-sgRNA) was diluted to a 35 µl solution with RNase-free water. Then 15 µl of 1.33 M stock of **2** in DMSO was added to the RNA solution. The mixture was incubated at 37 °C for 4 h.

To generate intermediately (~50%) **3**-cloaked RNA, 500 ng of RNA (tRF-3005 RNA) was diluted to an 8 µl solution with RNase-free water. Then 2 µl of 2 M stock of **3** in DMSO was added to the RNA solution. The mixture was incubated at room temperature for 4 h.

To generate intermediately (~50%) **4**-cloaked RNA, 500 ng of RNA (tRF-3005 RNA, eGFP-mRNA, EMX1-sgRNA, d2GFP-mRNA or total cellular RNA) was diluted to an 8 µl solution containing 700 mM HEPES (pH 7.3) and chilled on ice for >5 min. Then 2 µl of 500 mM stock of **4** in DMSO was added to the RNA solution. The mixture was incubated at 4 °C for 2.5 h. To generate extensively (>90%) **4**-cloaked RNA (tRF-3005 RNA or EMX1-sgRNA), 2.5 µg of RNA was diluted to a 40 µl solution containing 700 mM HEPES (pH 7.3) and chilled on ice for >5 min. Then 10 µl of 2 M stock of **4** in DMSO was added to the RNA solution. The mixture was incubated at 4 °C for 2.5 h.

To generate intermediately (~50%) cloaked RNA from **5**–**7**, 1.5 µg of RNA (tRF-3005 RNA, eGFP-mRNA, EMX1-sgRNA or d2GFP-mRNA) was diluted to an 18 µl solution with RNase-free water and chilled on ice for >5 min. Then 9 µl of 2 M stock of 5–7 in DMSO was added to the RNA solution. The mixture was incubated at 4 °C for 4 h.

Screening of non-basic nucleophiles for RNA uncloaking

First, 5 µl of cloaked tRF-3005 RNA (~15 µM) was mixed with 3 µl of 3.3 × reaction buffer (165 mM Tris, pH 7.5). Then 2 µl of reversal solution in water was added. This contained 250 mM of non-basic nucleophiles including potassium iodide (KI, in water), sodium thiocyanate (NaSCN, in water), 2-hydrazinobenzoic acid (in DMSO), methoxyamine hydrochloride (in DMSO), histidine (in water), sodium 3-(diphenylphosphino) benzenesulfonate (TPPMS, in water), tris(hydroxypropyl)phosphine (THPP, in water), 1-methylimidazole (in DMSO), DABCO (in water), Tris (pH 7.5), *N*-(3-aminopropyl)-imidazole (in DMSO), sodium cyanate (NaCN, in water) and 4-dimethylaminopyridine (in water). The resulting solution was incubated at 37 °C for 2 h. The RNA was purified by precipitation with ethanol according to the protocol described above. Then 7 µl of RNase-free water was added to dissolve the resulting RNA pellet and reconstitute the RNA solution. The number of remaining 2′-acyl adducts was determined using MALDI–TOF analysis. Reactions were performed once for each condition.

RNA uncloaking

To uncloaked total cellular RNA, 1 µg of **4**-cloaked isolated cellular RNA was diluted to 10 µl with RNase-free water. Then 10 µl of 100 mM Tris (pH 7.5) was added to the reaction mixture. The resulting solution was incubated at 37 °C for 24 h. Upon completion, the uncloaked total cellular RNA was used in the RT-qPCR experiments without further purification.

To uncloak **4**-cloaked RNA, 100 ng of **4**-cloaked eGFP-mRNA was diluted to 5 µl with RNase-free water. Then 5 µl of 100 mM or 400 mM Tris (pH 7.5) was added to the reaction mixture. The resulting solution was incubated at 37 °C for 24 h. Upon completion, the solution was used in the following in vitro translation experiments without further purification.

To uncloak **5**-/**6**-/**7**-cloaked RNA, 1 µg of cloaked RNA was first diluted to a 14 µl solution with water, then mixed with 5 µl of 250 mM

Tris (pH 7.5), 5 µl of 250 mM DABCO and 1 µl of RiboLock. The resulting solution was incubated at 37 °C for 11 h and then used in CRISPR-Cas9 experiments without further purification.

Accelerated mRNA ageing experiments

Two model long mRNAs (eGFP-mRNA and Fluc-mRNA) were used to evaluate the thermal stability of cloaked RNA. First, 50 µl of a solution containing 10 ng µl^{-1} of mRNA species in RNase-free water was incubated in a sealed RNase-free PCR tube at 37 °C. After the desired time, 3 µl of the mRNA solution was collected at each time point and RNA integrity was analysed by CE on Agilent RNA 6000 Pico Chips using an Agilent 2100 Bioanalyzer. CE data were processed and visualized using 2100 Expert software (Agilent). CE traces are shown in Figs. 1 and 2. Note: cloaking with **1** and **4** significantly reduces the electrophoretic mobility of RNA in the CE analysis; thus **1**- and **4**-cloaked RNAs have augmented apparent sizes in CE traces.

Predicting 'hotspots' of RNA degradation

Susceptibility to thermal degradation of each nucleotide in eGFP-mRNA's open reading frame was calculated computationally using the DegScore algorithm[7]. The secondary structure of eGFP-mRNA was first calculated using Vienna RNAfold. The RNA sequence and the optimal secondary structure in dot-bracket notation were then used to compute the DegScore for each nucleotide of eGFP-mRNA's open reading frame using the DegScore software (https://github.com/eternagame/DegScore). The DegScore was then divided by a factor of 100 to scale between 0 and 1.

In-line sequencing to characterize degradation site

A solution that contained 500 ng of degraded eGFP-mRNA, 2 pmol of RT primer (/5′-HEX/AGC TTG TGC CCC AGG ATG) and 10 mM dNTP was incubated at 65 °C for 5 min and then immediately chilled on ice for 2 min. Next, 2 µl of 5 × First-Strand Buffer, 1 µl of 0.1 M dithiothreitol, 0.5 µl of RNaseOUT and 0.5 µl of SuperScript II (200 U µl^{-1}) were added to the mixture. The reaction mixture was incubated at 25 °C for 10 min, 42 °C for 50 min and then 52 °C for 50 min. The resulting reaction mixture was used directly for DNA fragment analysis on a GeneScan-500 DNA. Data were analysed using Peak Scanner Software 2.

Determining deamination of nucleobases

First, 2 µg of poly(dA)5 or poly(dC)5 was incubated in RNase-free water for 14 days at an elevated temperature (37 °C). The solution was then subjected to digestion with Nucleoside Digestion Mix (purchased from NEB) following the manufacturer's protocol. The digested nucleosides were analysed using HPLC using dA, dC, dU and dI as standards. Eluent: 1% of methanol in 10 mM ammonium acetate buffer (pH 4.5) was used for 5 min. This was gradually increased to 30% of methanol over 32 min and maintained for 10 min.

Determining RNA enzymatic stability of EMX1-sgRNA

Protection of RNA from RNase T1. First, 100 ng of EMX1-sgRNA (unmodified or cloaked, 2 µl of 50 ng µl^{-1}) was diluted with 6 µl of reaction buffer (50 mM Tris (pH 7.5) plus 1 mM EDTA). To this was added 2 µl of a 5 × solution of RNase T1 (0.5 U µl^{-1}) in 50 mM Tris (pH 7.5) containing 1 mM EDTA. The solution was incubated at 37 °C for 9 min.

Protection of RNA from FBS. First, 100 ng of EMX1-sgRNA (unmodified or cloaked, 2 µl of 50 ng µl^{-1}) was diluted with 8 µl of 1 × PBS (pH 7.4) containing 0.5% FBS (v/v). The resulting solution was incubated at 37 °C for 2 min. Upon completion, the reaction mixture was immediately mixed with 10 µl of RNA Gel Loading dye (2×) and boiled at 95 °C for 2 min. Samples were then resolved using 6% denaturing polyacrylamide gel electrophoresis (PAGE). The gel was stained with 1 × SYBR Gold Nucleic Acid Gel Stain for 3 min and imaged using a Typhoon 9410 gel scanner (laser wavelength of 488 nm). The images were visualized and processed using ImageStudioLite software.

Isolation of total cellular RNA

HEK293 cells were grown on 15-cm plates in DMEM supplemented with 10% FBS until 90% confluence. The cells were washed with 10 ml of PBS once, then resuspended in 500 µl of PBS and lysed with 6 ml of Trizol LS by vortexing. Then 1.2 ml of chloroform was added. The resulting mixture was vortexed and incubated at room temperature for 5 min, followed by centrifugation at 2,500*g* for 15 min at 4 °C. The aqueous phase was then mixed with 1 × volume of 96% ethanol and purified using a Quick-RNA MidiPrep Kit with gDNA digestion according to the manufacturer's protocol.

RT-qPCR analysis of isolated total cellular RNA

The reverse transcription was performed with isolated total cellular RNA with or without cloaking. As an internal control, 100 pg of eGFP-mRNA (5-methoxyuridine-modified (5moU)) was added to each 500 ng of cellular RNA immediately before reverse transcription. First, 1 µl of RNA (500 ng µl^{-1}) was mixed with 1 µl of 50 µM oligo(dT)$_{18}$ primer, 1 µl of 10 mM dNTP mix and 10 µl of RNase-free water. The solution was incubated at 65 °C for 5 min, then immediately cooled on ice for >1 min. Next, 4 µl of RT buffer (5×), 1 µl of 0.1 M dithiothreitol, 1 µl of RiboLock and 1 µl of SuperScript III (200 U µl^{-1}) were added to the solution. The reaction mixture was incubated at 50 °C for 60 min and then the reaction was terminated by heating at 70 °C for 15 min. After cooling to 37 °C, 1 µl of RNase H (5 U µl^{-1}) was added. The resulting solution was then incubated at 37 °C for 20 min and used for qPCR without further purification.

Next, the qPCR analyses were performed using Luna Universal qPCR Master Mix (NEB, M3003) on a StepOnePlus Real-Time PCR System. First, 1 µl of complementary DNA product was mixed with 10 µl of Luna Universal qPCR Master Mix, 8 µl of water and 1 µl of a solution containing 5 µM forward primer and 5 µM reverse primer. Information about the primer sequences and amplicons for qPCR analyses of TBP, PPIE and PSMB6 are listed in Supplementary Tables 1 and 3. qPCR was performed using the following programme: initial denaturation for 60 s at 95 °C; 40 cycles of alternating denaturation (15 s at 95 °C) and extension (30 s at 60 °C). The ΔCt value was calculated to characterize the reverse transcription efficiency of each transcript as follows: the Ct value of each target was normalized to the Ct value of the internal control eGFP-mRNA (5moU) using the following equation: ΔCt (target) = Ct (target) − Ct (eGFP-mRNA (5moU)). ΔCt values are shown as mean ± s.e.m. (n = 3 of three biologically independent experiments).

In vitro translation of eGFP-mRNA

In vitro translation experiments were performed with eGFP-mRNA in wheat germ extract. First, 8 µl of 12.5 ng µl^{-1} eGFP-mRNA (100 ng in total) was added to a 384-well microplate (Greiner Bio-One, 781900). To it was added 12.5 µl of wheat germ extract (Promega, L4380), 0.5 µl of RNasin Plus RNase inhibitor (Promega, N2611), 2.0 µl of Complete Amino Acid mix (Promega, L4461) and 2.0 µl of 1 M KOAc. The resulting solution was mixed by gentle pipetting and then incubated at 25 °C for 90 min. After incubation, the green fluorescence signal was measured using a Fluoroskan Ascent FL microplate fluorometer (Excitation: 485 nm/Emission: 538 nm).

Cas9-mediated double-stranded DNA cleavage with EMX1-sgRNA

CRISPR-Cas9 experiments were performed with EMX1-sgRNA, PCR amplification products of genomic EMX1 and Cas9 nuclease. EMX1 double-stranded DNA was generated by PCR amplification of the genomic EMX1 according to previously reported protocols[52] (see Supplementary Table 2 for related oligonucleotide sequences). First, 1 µl of 50 ng µl^{-1} EMX1-sgRNA was mixed with 5.67 µl of water, 1 µl of 10 × NEbuffer 3.1 and 1.33 µl of 1 µM Cas9 Nuclease (*Streptococcus pyogenes*). The resulting solution was incubated at 25 °C for 10 min. After incubation, 1 µl of 50 ng µl^{-1} of EMX1 double-stranded DNA substrate

was added and the reaction mixture was then incubated at 37 °C for 2 h. After the reaction, 2 µl of 6× Orange Gel loading dye was added. The samples were resolved by electrophoresis on a 1% agarose gel containing 1 × SYBR Gold Nucleic Acid stain. The gel was imaged using a Typhoon 9410 gel scanner (laser wavelength of 488 nm). The gel images were visualized and processed using ImageStudioLite software.

Fluorescence-activated cell sorting analysis

HeLa cells were seeded on a 12-well plate and grown to ~40% confluency in DMEM supplemented with 10% FBS in a humidified incubator at 37 °C with 5% CO_2. Cells were transfected with 1 µg of eGFP-mRNA species per well using 3 µl of Lipofectamine MessengerMAX reagent according to the manufacturer's protocol. After 24 and 48 h, cells were washed once with warm Dulbecco's phosphate-buffered saline and detached from wells by treatment with 100 µl of trypsin-EDTA (0.25%). The cells were then mixed with 1 ml of DMEM and centrifuged at 350*g* for 5 min. Next, the pellet of cells was resuspended in 1 ml of 4% paraformaldehyde in PBS and fixed for 20 min at 4 °C in the dark. Finally, the cells were centrifuged at 350*g* for 5 min and resuspended in 180 µl of PBS containing 2% FBS. Fluorescence-activated cell sorting analyses were performed on a NovoCyte Quanteon flow cytometer with a blue laser at 488 nm (100 mW) and a B530 detector and 25,000 cells were recorded for each condition for the analysis. Data were analysed using FlowJo V10. See Supplementary Fig. 13 for the gating strategy.

Confocal microscopy of eGFP-mRNA translation

HeLa cells were seeded onto a FluoroDish with a 10-mm cover glass bottom (World Precision Instruments, FD3510B100) at a density of 5.0×10^5 cells and incubated overnight in 100 µl of DMEM supplemented with 10% FBS at 37 °C with 5% CO_2. For each FluoroDish, the cells were transfected with 100 ng of eGFP-mRNA species with 0.3 µl of Lipofectamine MessengerMAX transfection reagent according to the manufacturer's protocol. After 24 or 48 h, the medium was removed, then the cells were washed 3 times with PBS and fixed with 200 µl of 4% paraformaldehyde for 20 min at room temperature. After fixation, cells were washed 3 times with PBS and then stained with 10 µg ml^{-1} Hoechst 33342 for 30 min at room temperature. After staining, the cells were washed 3 times with PBS, then mounted on an inverted Zeiss LSM 780 confocal laser scanning microscope equipped with a 34-channel spectral array with laser lines at 450, 458, 488, 514, 561, 594 and 633 nm. This was carried out at the Cell Science Imaging Facility at Stanford University. A 25× oil immersive objective was employed for the imaging. The nucleus stained with Hoechst 33342 was imaged with a 405 nm laser with a 415–470 nm emission filter set and GFP was imaged with a 488 nm laser with a 500–615 nm emission filter set. Images were processed and analysed in ImageJ software.

Fluorimeter-based assays monitoring mRNA translation kinetics

On a 96-well plate, 0.01×10^6 cells were seeded into each well in 100 µl of FluoroBrite DMEM (Thermo Scientific, A1896701) containing 10% FBS. In each well, cells were transfected by 100 ng of mRNA with 0.3 µl of Lipofectamine MessengerMAX reagent in serum-free FluoroBrite DMEM according to the manufacturer's protocol. Then, the transfection reagents were removed by replacing the medium with 180 µl of fresh FluoroBrite DMEM containing 10% FBS. GFP translation was monitored using a microplate reader (Tecan Infinite M1000) over time. GFP fluorescence was detected using 488 nm/519 nm for the excitation/emission wavelengths.

Quantification and statistical analysis

For all statistical tests (unless otherwise noted), two-tailed unpaired Student's *t*-tests were used to compare means between two samples. Significance is denoted as follows: * = $P < 0.05$, ** = $P < 0.01$, *** = $P < 0.001$ and **** = $P < 0.0001$. Statistical tests were performed using GraphPad Prism9 software. Quantifications shown are mean ± s.e.m. unless otherwise stated.

Reporting summary

Further information on research design is available in the Nature Portfolio Reporting Summary linked to this article.

Data availability

All relevant data supporting the findings of this study are available within the article and supplementary information. The characterization data of all organic compounds are provided within the supplementary information. All reagents generated in this study are available from the corresponding author upon reasonable request. Data used for this paper are also available via figshare at https://figshare.com/articles/dataset/NCHEM-22030547_source_data/19555132. Source data are provided with this paper.

References

52. Gu, C. et al. Chemical synthesis of stimuli-responsive guide RNA for conditional control of CRISPR-Cas9 gene editing. *Chem. Sci.* **12**, 9934–9945 (2021).
53. Warren, L. et al. Highly efficient reprogramming to pluripotency and directed differentiation of human cells with synthetic modified mRNA. *Cell Stem Cell* **7**, 618–630 (2010).

Acknowledgements

This work was supported by a grant from the US National Institutes of Health GM127295 to E.T.K. The funder had no role in study design, data collection and analysis, decision to publish, or preparation of the manuscript. We thank K. Fukui and other staff at the Stanford PAN facility for performing BioAnalyzer QC. We thank Stanford Shared FACS Facility (SSFF) for the flow cytometry analysis. We thank T. McLaughlin in the Vincent Coates Foundation Mass Spectrometry Laboratory, Stanford University Mass Spectrometry (RRID:SCR_017801) for acquiring the HRMS data. We also thank T. Trinh for performing circular dichroism measurements and L. Zheng for the helpful discussion.

Author contributions

L.F. and E.T.K. conceived the project and designed the experiments. L.F. performed the experiments and data analysis. L.X. performed the Cas9-mediated DNA cleavage assay. Y.W.J. collected and analysed the confocal microscopy data. E.T.K. supervised the work. L.F. and E.T.K. wrote the paper, with input from all authors.

Competing interests

Stanford University has filed a patent application (PCTUS2023/010686) based on the RNA cloaking and uncloaking reagents and methods described in this work, in which L.F. and E.T.K. are named as inventors. The other authors declare no competing interests.

Additional information

Extended data is available for this paper at https://doi.org/10.1038/s41557-023-01246-6.

Supplementary information The online version contains supplementary material available at https://doi.org/10.1038/s41557-023-01246-6.

Correspondence and requests for materials should be addressed to Eric T. Kool.

Peer review information *Nature Chemistry* thanks Ashwani Sharma, Joanna Sztuba-Solinska, Wen Zhang and the other, anonymous, reviewer(s) for their contribution to the peer review of this work.

https://doi.org/10.1038/s41557-023-01246-6

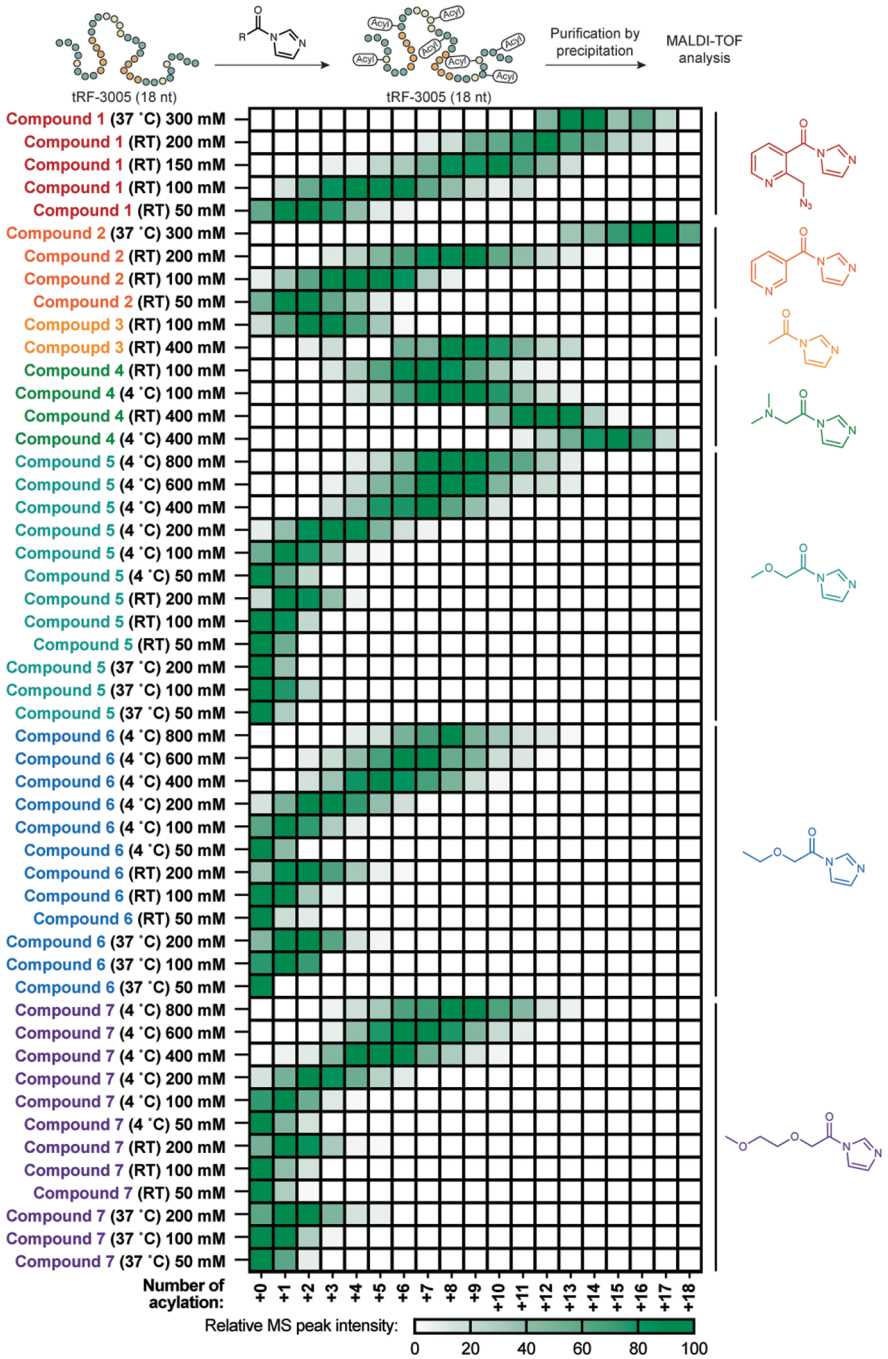

Extended Data Fig. 1 | Reaction conditions of RNA cloaking with acylimidazole reagents. A heatmap shows reaction conditions for each acylimidazole reagent (1-7) required to introduce the desired level of RNA cloaking using a model 18nt tRF-3005 RNA. The X-axis indicates the number of 2′-acyl adducts per RNA molecule identified by MALDI-TOF. The color intensity of each cell represents the mass intensity of the acyl adduct peak (numbers at bottom show numbers of acyl adducts for the model RNA strand). See Supplementary Table 1 for quantification.

https://doi.org/10.1038/s41557-023-01246-6

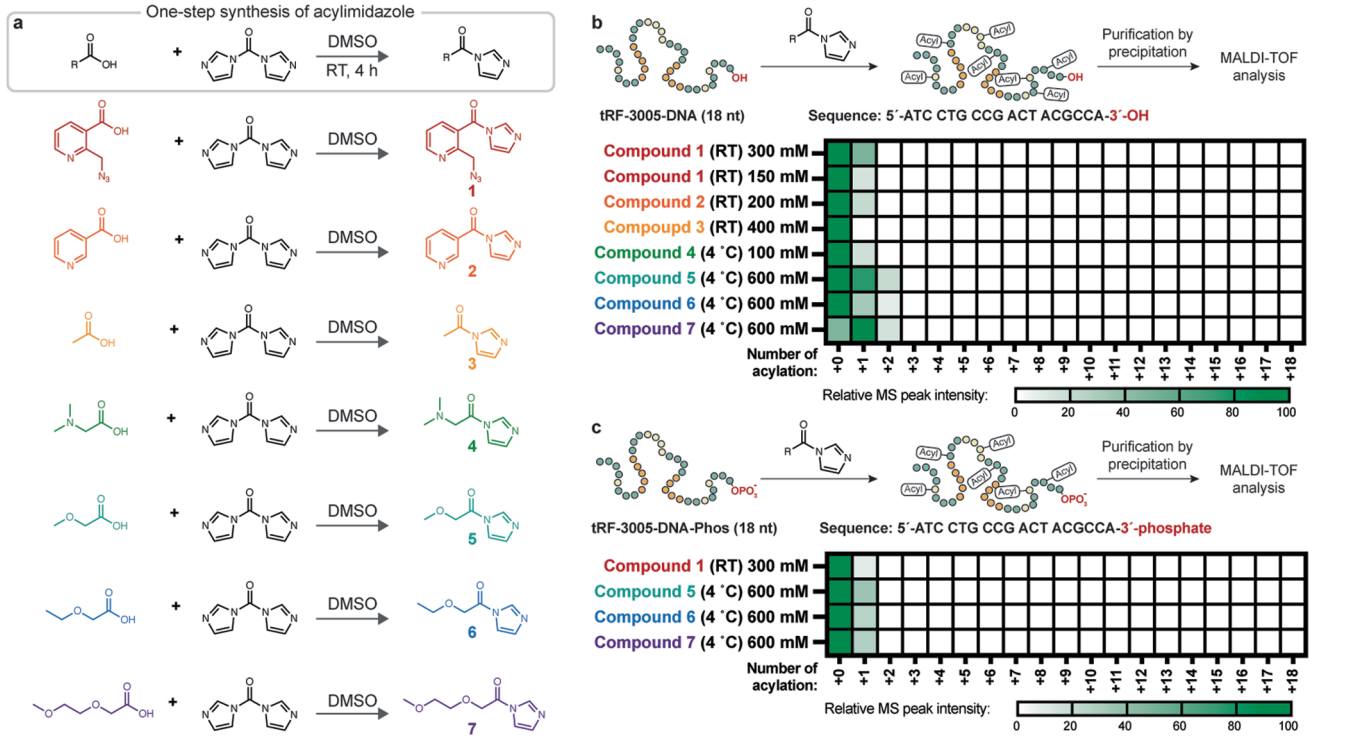

Extended Data Fig. 2 | One-step synthesis of acylimidazoles for selectively 2′-OH acylation. a, Schematic for one-step synthesis of acylimidazole reagents. **b**-**c**, Comparisons of RNA and DNA with the same sequence (tRF-3005-DNA and tRF-3005-DNA-Phos) after reacting with **1**-**7** show that reaction occurs entirely or almost entirely at 2′-OH groups rather than nucleobases or phosphodiester bonds. **b**, Number of acyl adducts on tRF-3005-DNA (18nt) upon treatment with acylimidazole reagents **1**-**7**. tRF-3005-DNA contains an unmodified 3′-OH (Sequence: 5′-ATC CTG CCG ACT ACG CCA-3′-OH). **c**, Number of acyl adducts on tRF-3005-DNA-Phos (18nt) upon treatment with acylimidazole reagents **1**, **5**, **6**, and **7**. tRF-3005-DNA-Phos contains a blocked 3′-end by 3′-phosphorylation (Sequence: 5′-ATC CTG CCG ACT ACG CCA-3′-phosphate). The X-axis shows the number of acyl adducts per DNA identified by MALDI-TOF. The color intensity of each cell represents the mass intensity of the acyl adduct peak.

https://doi.org/10.1038/s41557-023-01246-6

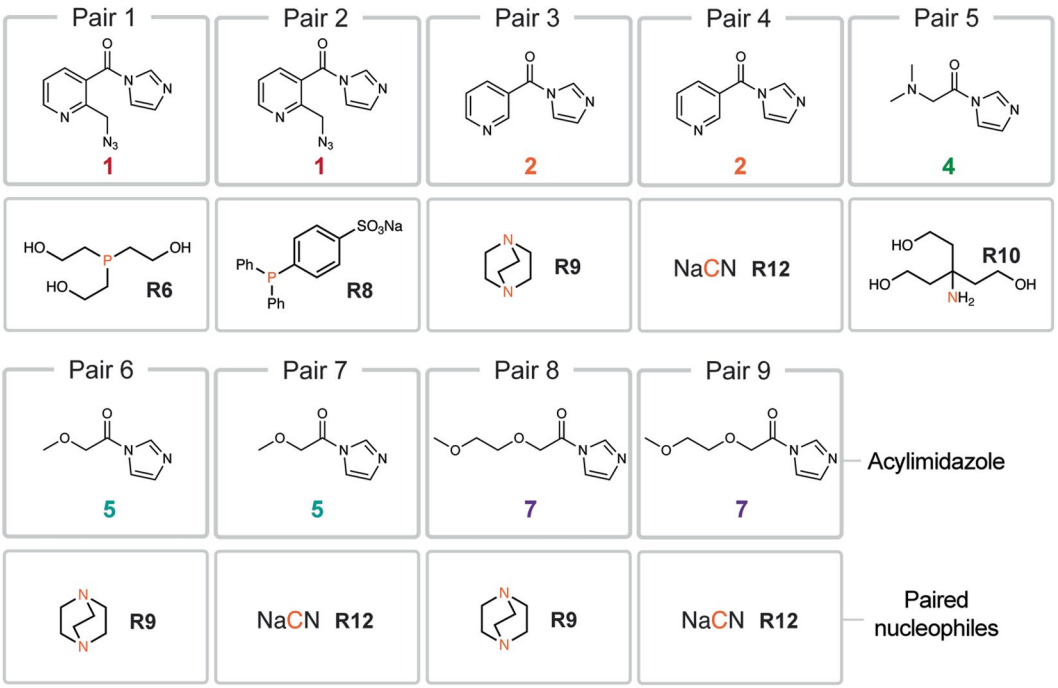

Extended Data Fig. 3 | Sensitive acylimidazole-nucleophile pairs. A summary of sensitive acylimidazole-nucleophile pairs that afford >50% hydrolysis of 2′-acyl adducts within 2 hours. The electrophilic centers are coloured orange.

https://doi.org/10.1038/s41557-023-01246-6

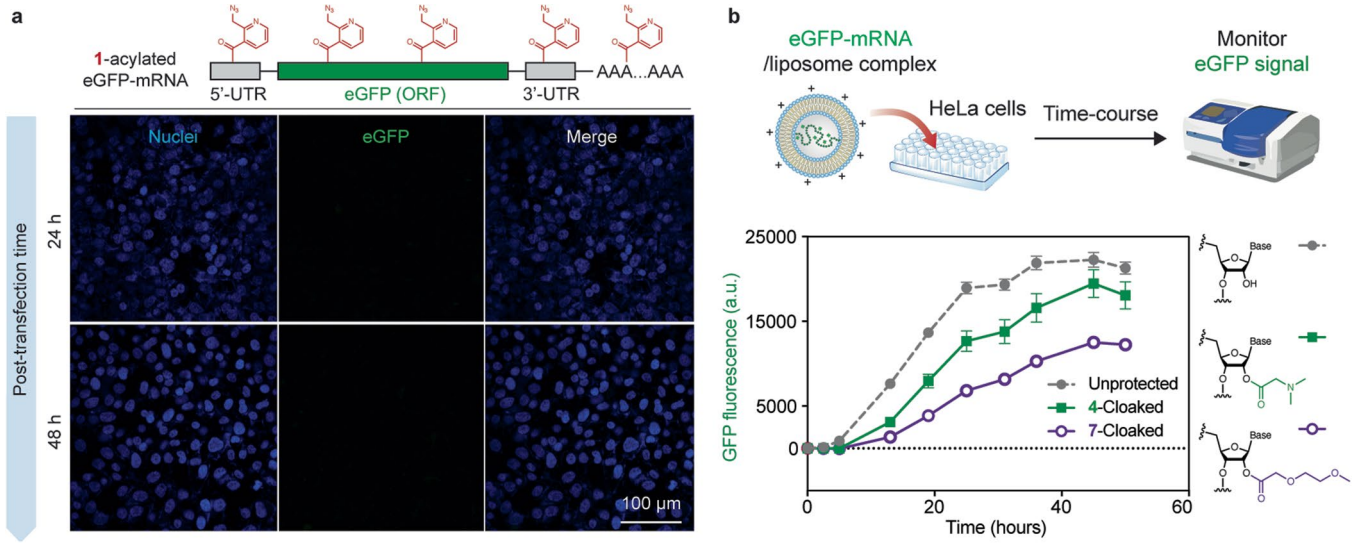

Extended Data Fig. 4 | Spontaneous RNA uncloaking restores mRNA translation in human cells. a, Representative single-blind fluorescence micrographs of HeLa cells transfected with **1**-cloaked eGFP-mRNA showing strongly inhibited mRNA translation after 24 or 48 h. Each condition was imaged at areas that contain more than 50 cells over two independent experiments. **b**, Time-course plot showing **7**-cloaked eGFP-mRNA (~50% of 2′-hydroxyls acylated) translates in HeLa cells. Its translation kinetics were compared to unprotected or equimolarly **4**-cloaked eGFP-mRNA. Data represent mean ± s.e.m., $n = 3$ per group from three biologically independent experiments.

nature portfolio

Corresponding author(s): Eric T. Kool

Last updated by author(s): Feb 8, 2023

Reporting Summary

Nature Portfolio wishes to improve the reproducibility of the work that we publish. This form provides structure for consistency and transparency in reporting. For further information on Nature Portfolio policies, see our Editorial Policies and the Editorial Policy Checklist.

Statistics

For all statistical analyses, confirm that the following items are present in the figure legend, table legend, main text, or Methods section.

n/a	Confirmed	
☐	☒	The exact sample size (*n*) for each experimental group/condition, given as a discrete number and unit of measurement
☐	☒	A statement on whether measurements were taken from distinct samples or whether the same sample was measured repeatedly
☐	☒	The statistical test(s) used AND whether they are one- or two-sided *Only common tests should be described solely by name; describe more complex techniques in the Methods section.*
☒	☐	A description of all covariates tested
☒	☐	A description of any assumptions or corrections, such as tests of normality and adjustment for multiple comparisons
☐	☒	A full description of the statistical parameters including central tendency (e.g. means) or other basic estimates (e.g. regression coefficient) AND variation (e.g. standard deviation) or associated estimates of uncertainty (e.g. confidence intervals)
☐	☒	For null hypothesis testing, the test statistic (e.g. *F*, *t*, *r*) with confidence intervals, effect sizes, degrees of freedom and *P* value noted *Give P values as exact values whenever suitable.*
☒	☐	For Bayesian analysis, information on the choice of priors and Markov chain Monte Carlo settings
☒	☐	For hierarchical and complex designs, identification of the appropriate level for tests and full reporting of outcomes
☒	☐	Estimates of effect sizes (e.g. Cohen's *d*, Pearson's *r*), indicating how they were calculated

Our web collection on statistics for biologists contains articles on many of the points above.

Software and code

Policy information about availability of computer code

Data collection	Softwares used for data collection are all from the instrument manufacturers. VNMRJ (Version 4.2) was used on the NMR. Ascent software (Version 2.6) was used on the plate reader. The flexControl (Version 3.4) was used on the MALDI-TOF. Zeiss ZEN (Version: Zen 2.3 SP1 FP3 (black) 64 bit, LSM 780 14.0) was used on the confocal microscope. NovoExpress (Version 1.6.1) was used on NovoCyte Quanteon Flow Cytometer. DNA fragment analysis was performed on a GeneScan-500 DNA.
Data analysis	GraphPad Prism 9 (Version 9.5.0) was used for common plots. ImageJ (Version 2.3.0/1.53f) was used for microscope image processing. MestReNova (Version 14.2.3-29241) was used for NMR and MALDI-TOF data processing. ImageStudioLite (Version 5.2.5) was for gel image processing. Flow cytometry data was analyzed with FlowJo V10 (Version 10.8.1). Capillary electrophoresis data was analyzed with 2100 expert software (Version B.02.11.SI811). DNA fragment analysis data were analyzed with Peak Scanner Software 2 (Version 2.0).

For manuscripts utilizing custom algorithms or software that are central to the research but not yet described in published literature, software must be made available to editors and reviewers. We strongly encourage code deposition in a community repository (e.g. GitHub). See the Nature Portfolio guidelines for submitting code & software for further information.

Data

Policy information about availability of data

All manuscripts must include a data availability statement. This statement should provide the following information, where applicable:

- Accession codes, unique identifiers, or web links for publicly available datasets
- A description of any restrictions on data availability
- For clinical datasets or third party data, please ensure that the statement adheres to our policy

The authors declare that all relevant data supporting the findings of this study are available within the article and Supplementary Information. The characterization data of all organic compounds are provided within the Supplementary Information. All reagents generated in this study are available upon reasonable request. Source data are provided with this paper. Data used for this paper are also available at https://figshare.com/articles/dataset/NCHEM-22030547_source_data/19555132 at Figshare.

Human research participants

Policy information about studies involving human research participants and Sex and Gender in Research.

Reporting on sex and gender	N/A
Population characteristics	N/A
Recruitment	N/A
Ethics oversight	N/A

Note that full information on the approval of the study protocol must also be provided in the manuscript.

Field-specific reporting

Please select the one below that is the best fit for your research. If you are not sure, read the appropriate sections before making your selection.

☒ Life sciences ☐ Behavioural & social sciences ☐ Ecological, evolutionary & environmental sciences

For a reference copy of the document with all sections, see nature.com/documents/nr-reporting-summary-flat.pdf

Life sciences study design

All studies must disclose on these points even when the disclosure is negative.

Sample size	In vitro RNA enzymatic degradation assays were independently conducted at least three times (n≥3). Cellular experiments involving human cells were conducted in three biologically independent replicates. In vitro RNA accelerated aging by heating is a highly reproducible biochemical reaction as shown in European Journal of Human Genetics volume 22, pages 379–385 (2014), therefore the sample size is (n=2) unless otherwise stated in the manuscript.
Data exclusions	No data were excluded from the analyses.
Replication	All attempts at replication were successful. In vitro RNA enzymatic degradation assays were independently repeated at least three times (n≥3) and showed similar results. Experiments involving human cells were conducted in three biologically independent replicates that showed similar results. In vitro RNA accelerated aging by heating was independently conducted twice and showed similar results.
Randomization	All samples and cells were randomly allocated into experimental groups.
Blinding	Confocal imaging was performed in a single-blind manner to avoid biases. Blinding was not required for the other experiments, where none of the methods for measurement and analysis were susceptible to personal prejudice.

Reporting for specific materials, systems and methods

We require information from authors about some types of materials, experimental systems and methods used in many studies. Here, indicate whether each material, system or method listed is relevant to your study. If you are not sure if a list item applies to your research, read the appropriate section before selecting a response.

Materials & experimental systems

n/a	Involved in the study
☒	☐ Antibodies
☐	☒ Eukaryotic cell lines
☒	☐ Palaeontology and archaeology
☒	☐ Animals and other organisms
☒	☐ Clinical data
☒	☐ Dual use research of concern

Methods

n/a	Involved in the study
☒	☐ ChIP-seq
☐	☒ Flow cytometry
☒	☐ MRI-based neuroimaging

Eukaryotic cell lines

Policy information about cell lines and Sex and Gender in Research

Cell line source(s)	HEK293, HeLa, and SW480 lines were obtained from ATCC.
Authentication	The morphology check by microscope was performed to authenticate the cell lines.
Mycoplasma contamination	Cell lines were not tested for mycoplasma contamination.
Commonly misidentified lines (See ICLAC register)	None.

Flow Cytometry

Plots

Confirm that:

☒ The axis labels state the marker and fluorochrome used (e.g. CD4-FITC).

☒ The axis scales are clearly visible. Include numbers along axes only for bottom left plot of group (a 'group' is an analysis of identical markers).

☒ All plots are contour plots with outliers or pseudocolor plots.

☒ A numerical value for number of cells or percentage (with statistics) is provided.

Methodology

Sample preparation	HeLa cells were obtained from ATCC. The treated cells were disassociated from culture dishes by treatment with trypsin-EDTA, and fixed with 4% paraformaldehyde in PBS before being tested on the flow cytometer.
Instrument	NovoCyte Quanteon Flow Cytometer, Agilent, USA
Software	Data were collected with NovoExpress software, and processed with FloJo software.
Cell population abundance	For each measurement, 25,000 cells were recorded. All the recorded cells were shown in the dot plots.
Gating strategy	The gating strategy was established on the data collected from cells transfected with an equal amount of unprotected eGFP-mRNA in the control groups, and applied to the experimental groups. The gating strategies are shown in the Supplementary Information Fig. 13.

☒ Tick this box to confirm that a figure exemplifying the gating strategy is provided in the Supplementary Information.